ATMIRE

Title	Analysis of passive earth pressure and slope stability reliability by the random finite element method, The
Item Type	Text
Authors	Ziemann, Heidi R.
Publisher	Colorado School of Mines. Arthur Lakes Library
Rights	Copyright of the original work is retained by the author.
Download date	2026-11-28 09:45:14
Link to Item	https://hdl.handle.net/11124/170715

THE ANALYSIS OF PASSIVE EARTH PRESSURE AND SLOPE STABILITY RELIABILITY BY THE RANDOM FINITE ELEMENT METHOD

by

Heidi R. Ziemann

A thesis submitted to the Faculty and the Board of Trustees of the Colorado School of Mines in partial fulfillment of the requirements for the degree of Master of Science (Engineering Systems).

Golden, Colorado

Date 11.14.05

Signed: _____
Heidi R. Ziemann

Approved: _____
Dr. D. V. Griffiths
Professor of Engineering
Thesis Advisor

Golden, Colorado

Date 11/14/05

_____
Dr. Dave Muñoz
Interim Division Director
Division of Engineering

ABSTRACT

The investigation of the estimated probability of failure for a soil with spatially random shear strength parameters characterized by a mean, coefficient of variation and spatial correlation length is presented for both a passive earth pressure analysis and a slope stability analysis. The estimated probability of failure is determined using a First Order Second Moment Method and the Random Finite Element Method. The First Order Second Moment Method is modified to include spatial correlation length by locally averaging the soil strength parameters over a predefined failure surface. The estimated probability of failure is determined using a performance function based on traditional equilibrium theory and a probability density function assumed to be characterized by a lognormal distribution. The Random Finite Element Method incorporates random field theory with an elasto-viscoplastic finite element algorithm in a Monte Carlo framework to determine the estimated probability of failure. A comparison of the two methods is presented.

TABLE OF CONTENTS

ABSTRACT iii
TABLE OF CONTENTS iv
LIST OF FIGURES vii
LIST OF TABLES xi
LIST OF TABLES xi
ACKNOWLEDGEMENTS xii
DEDICATION xiii
1. INTRODUCTION 1
1.1 Problem and Background 1
1.2 Previous Work 2
1.3 Present Approach 4
2. OVERVIEW OF THE FINITE ELEMENT METHOD 6
2.1 Soil Model 6
2.2 Viscoplastic Algorithm 9
2.3 Passive Earth Pressure Analysis 11
2.3.1 Displacement Control Method 12
2.4 Slope Stability Analysis 14
2.4.1 Shear Strength Reduction Method 15
3. THE FIRST ORDER SECOND MOMENT (FOSM) METHOD 17
3.1 Traditional Method for a Single Random Variable 17
3.2 Modified Method for a Single Random Variable in 1-D 22
3.2.1 Variance Reduction Over a Line 22
4. THE RANDOM FINITE ELEMENT METHOD (RFEM) 26
4.1 Characterization of the Input Random Variable 26
4.2 Variance Reduction of Input Parameters 27

4.3 Simulation Via Local Average Subdivision 29
4.4 Monte Carlo Simulation 31

4.4.1 Influence of the Number of Monte Carlo Simulations 32

5. PASSIVE EARTH PRESSURE 35

5.1 Rankine Theory of Earth Pressure 36
5.2 First Order Second Moment (FOSM) Method 38

5.2.1 Variance Reduction due to Local Averaging 39
5.2.2 Design Reliability 40
5.2.3 FOSM Method Results 41

5.3 Random Finite Element Method 46

5.3.1 Design Reliability 47
5.3.2 Monte Carlo Results Based on Virtual Sampling 48

5.4 Comparison of the FOSM and the RFEM Methods 58

5.4.1 Influence of the Coefficient of Variation on Design Reliability 59
5.4.2 Influence of Spatial Correlation Length on Design Reliability. 61
5.4.3 Summary of Observations 63

6. SLOPE STABILITY 64

6.1 Traditional Slope Stability Equilibrium Methods 66

6.1.1 Bishop's Modified Method of Slices 66

6.2 First Order Second Moment (FOSM) Method 69

6.2.1 Variance Reduction Due to Local Averaging 71
6.2.2 Design Reliability 73
6.2.3 FOSM Method Results 73

6.3 Random Finite Element Method (RFEM) 78

6.3.1 Design Reliability 78
6.3.2 Monte Carlo Results 79

6.4 Comparison of the FOSM and the RFEM Methods 81

6.4.1 Summary of Observations 84

7. CONCLUDING REMARKS AND FUTURE WORK 88

7.1 Concluding Remarks 88
7.2 Suggestions for Future Work 89

7.2.1 Passive Earth Pressure 89
7.2.2 Slope Stability Analysis 90

REFERENCES CITED 91

LIST OF FIGURES

Figure 2.1: Elastic-Perfectly Plastic Soil Model 6

Figure 2.2: Mohr-Coulomb Failure Criterion 8

Figure 2.3: Rheological Model for 1-d Viscoplasticity 9

Figure 2.4: Mesh and Boundary Conditions for Passive Earth Pressure Analysis 12

Figure 2.5: Passive Force vs. Displacement Increment 14

Figure 2.6: Mesh and Boundary Conditions for Slope Stability Analysis 15

Figure 3.1: Normal PDF for $\mu_X = 100$ and $\sigma_X = 50$ 20

Figure 3.2: Lognormal PDF for μ_X =100 and σ_X=50 22

Figure 3.3: Variance Reduction Function, γ vs. α for Constant θ 24

Figure 4.1: Variance Reduction Function, γ vs. α for Constant $\theta_{\ln x}$ 28

Figure 4.2: Typical Random Fields in the RFEM Method 31

Figure 4.3: Typical random fields in the RFEM method for constant statistical input parameters μ_x, V_x and $\Theta_{\ln x}$ 32

Figure 4.4: Effect of the Number of Realizations on the Passive Force Statistics 33

Figure 4.5: Standard error versus probability of failure for 1000 Monte Carlo Realizations 34

Figure 5.1: Traditional failure plane 37

Figure 5.2: $\frac{\alpha\theta}{H}$ vs. Number of Subdivisions 39

Figure 5.3: Influence of number of subdivisions on local averaging: influence on the (a) mean and (b) standard deviation for $\Theta_{\ln \tan \phi'} = 1.0$ 40

Figure 5.4: Estimated probability of failure, p_f, that the true lateral passive load will be less than the factored predicted design load for $\Theta_{\ln \tan \phi'} = 1.0$ 42

Figure 5.5: Estimated probability of failure, p_f, that the true lateral passive load will be less than the factored predicted design load for $\Theta_{\ln \tan \phi'} = 1.0$ and *FOS=1.2.* 43

Figure 5.6: Estimated probability of failure, p_f, that the true lateral passive load will be less than the factored predicted design load for $V_{\tan \phi'} = 0.30$ 44

Figure 5.7: Estimated probability of failure, p_f, that the true lateral passive load will be less than the factored predicted design load for $V_{\tan \phi'} = 0.30$ and $\Theta_{\ln \tan \phi'} = \infty$ 45

Figure 5.8: Estimated probability of failure, p_f, that the true lateral passive load will be less than the factored predicted design load for $V_{\tan \phi'} = 0.30$ and *FOS=1.2.* 46

Figure 5.9: Estimated probability of failure, p_f, that the true lateral passive load will be less than the factored predicted design load for virtual sample point 1 for (a) $\Theta_{\ln \tan \phi'} = 0.05$, (b) $\Theta_{\ln \tan \phi'} = 0.2$, (c) $\Theta_{\ln \tan \phi'} = 2.0$, and (d) $\Theta_{\ln \tan \phi'} = 5.0$ 49

Figure 5.10: Estimated probability of failure, p_f, that the true lateral passive load will be less than the factored predicted design load for *FOS=1.2.* 50

Figure 5.11: Passive earth displacement for a soil friction angle realization, $V_{\tan \phi'} = 0.5$ and (a) $\Theta_{\ln \tan \phi'} = 0.05$, (b) $\Theta_{\ln \tan \phi'} = 0.5$, and (c) $\Theta_{\ln \tan \phi'} = 5.0$ 52

Figure 5.12: Contour of shear strain invariant for soil friction angle realization illustrated in figure 5.11 for (a) $\Theta_{\ln \tan \phi'} = 0.05$, (b) $\Theta_{\ln \tan \phi'} = 0.5$, and (c) $\Theta_{\ln \tan \phi'} = 5.0$ 53

Figure 5.13: (a) Passive earth displacement for a soil friction angle realization, $V_{\tan\phi'} = 0.5$ and $\Theta_{\ln\tan\phi'} = 0.5$, and (b) corresponding contour of shear strain invariant for a soil friction angle realization. 55

Figure 5.14: Estimated probability of failure, p_f, that the true lateral passive load will be less than the factored predicted design load for varying virtual sample point locations with *FOS=1.2* and (a) $\Theta_{\ln\tan\phi'} = 0.05$, (b) $\Theta_{\ln\tan\phi'} = 0.2$, (c) $\Theta_{\ln\tan\phi'} = 1.0$, and (d) $\Theta_{\ln\tan\phi'} = 5.0$. 57

Figure 5.15: Estimated probability of failure, p_f, that the true lateral passive load will be less than the factored predicted design for virtual samples located at (*H*/2, *H*/2) and (*H*, *H* /2) with *FOS=1.2*. 58

Figure 5.16: Estimated probability of failure, p_f, that the true lateral passive load will be less than the factored predicted design load with *FOS=1.2* and (a) $\Theta_{\ln\tan\phi'} = 0.05$, (b) $\Theta_{\ln\tan\phi'} = 0.2$, (c) $\Theta_{\ln\tan\phi'} = 1.0$, and (d) $\Theta_{\ln\tan\phi'} = 5.0$. 60

Figure 5.17: Estimated probability of failure, p_f, that the true lateral passive load will be less than the factored predicted design load with *FOS=1.2* and (a) $V_{\tan\phi'} = 0.20$, (b) $V_{\tan\phi'} = 0.30$, (c) $V_{\tan\phi'} = 0.50$. 62

Figure 6.1: Cohesive slope test problem 64

Figure 6.2: Bishop's Modified Method of Slice 67

Figure 6.3: Linear relationship between *FOS* and *C* for a cohesive slope with β = 26.67° and *D*=2. 68

Figure 6.4: Assumed Failure Circle with Example Subdivisions 70

Figure 6.5: $\alpha\theta$ vs. Number of Subdivisions 71

Figure 6.6: Influence of number of subdivisions on local averaging: influence on the (a) mean and (b) standard deviation for $\Theta_{\ln C} = 1.0$ 72

Figure 6.7: Estimated probability of failure, p_f vs. the coefficient of variation, V_C for (a) $\Theta_{\ln C} = 0.5$, (b) $\Theta_{\ln C} = 1.0$, (c) $\Theta_{\ln C} = 2.0$, and (d) $\Theta_{\ln C} = 5.0$. 74

Figure 6.8: Estimated probability of failure, p_f vs. the spatial correlation length , $\Theta_{\ln C}$ for (a) $V_C = 0.5$ and (b) $V_C = 1.0$. 76

Figure 6.9: Estimated probability of failure, p_f vs. the coefficient of variation, V_C for $\Theta_{\ln C} = \infty$. 77

Figure 6.10: Mesh Used for Random Finite Element Slope Stability Analysis ...78

Figure 6.11: Estimated probability of failure, p_f, vs. the coefficient of variation, V_C 79

Figure 6.12: Estimated probability of failure, p_f, vs. the spatial correlation length , $\Theta_{\ln C}$. 80

Figure 6.13: Estimated probability of failure, p_f vs. the coefficient of variation, V_C for (a) $\Theta_{\ln C} = 0.5$, (b) $\Theta_{\ln C} = 1.0$, (c) $\Theta_{\ln C} = 2.0$, and (d) $\Theta_{\ln C} = 4.0$ ...82

Figure 6.14: Estimated probability of failure, p_f vs. the coefficient of variation, V_C for (a) $V_C = 0.25$, (b) $V_C = 0.50$, (c) $V_C = 0.75$, and (d) $V_C = 1.0$. 83

Figure 6.15: (a) Soil shear strength realization grey scale plot, $V_C = 1.0$ and $\Theta_{\ln C} = 4.0$, and (b) corresponding contour of shear strain invariant at failure. 85

Figure 6.16: Contour of shear strain invariant at failure for different Monte Carlo realizations with $V_C = 0.25$ and $\Theta_{\ln C} = 4.0$ 86

LIST OF TABLES

Table 2.1: Six-Parameter Soil Model....7

Table 2.2: Failure Function Definition....8

Table 5.1: Parameters varied in study....36

Table 5.2: Location of virtual sample points in study....48

Table 6.1: Parameters varied in study....66

Table 6.2: *FOS* Assuming a Homogeneous Soil....68

ACKNOWLEDGEMENTS

With sincere appreciation I would like to recognize my advisor Dr. D. V. Griffiths whose mentoring was an integral part of my growth as a graduate student.

I would like to gratefully acknowledge my committee members, Dr. Ning Lu and Dr. Mike Mooney, for their willingness to help and the positive feedback they gave.

I would also like to thank my friends and family for their time and encouragement.

DEDICATION

This thesis is dedicated to Stacey Ronat. Without the support of this individual, I would never have pursued a Master's degree, completed the work required or be as happy every day.

My dearest thanks to you.

1. INTRODUCTION

1.1 Problem and Background

Traditionally, geotechnical analysis is performed assuming constant soil properties. The inherent variability of the soil is not modeled directly. To account for the variability, traditional theory applies a factor of safety to the results that were obtained using characteristic (e.g. mean) soil properties. The factor of safety that is applied is based on engineering judgment and experience. The same factor of safety is often applied, due to tradition or regulation, for similar geotechnical analyses regardless of the degree of uncertainty involved in its calculation (e.g Duncan 2000).

Probabilistic methods provide a scientific basis to quantify the effects of soil property variability and the degree of uncertainty. If it is assumed that the independent soil properties are random variables described by a mean, coefficient of variation, spatial correlation length, and a probability density function, the probability density function of the dependent variable can be estimated based on the input random variables. The output probability density function can then be used to define the reliability, the probability that failure will not occur, of the analysis considered. The word failure as used in the context of reliability includes catastrophic failure as well as unsatisfactory performance.

Reliability information provides several benefits in geotechnical engineering. Alternative designs can be evaluated by comparing probabilities of failure. As an example, different modes of failure could be investigated and the corresponding probabilities of failure compared. A traditional factor of safety approach would not provide adequate information as the same factor of safety for

different modes of failure may correspond to significantly different values of failure probability. Risk can be readily assessed and more economical designs incorporating acceptable risk, can be developed. The sensitivity of the design to a particular independent variable can be evaluated while providing insight into the value of increasing the quality of the variable in the design.

1.2 Previous Work

Uncertainty and reliability have been a topic in geotechnical engineering from its conception. They have also been a topic of controversy. Terzaghi (1929) emphasized the importance of understanding the impact of geological features that differ from the mean conditions. He criticized then current practice for trusting in purely statistical relations that have a wide range of deviation and the confidence engineers had in the obtained reliability results. He recommended that designers "assume...the most unfavorable possibilities". As a consequence of this work, progress in this area came to a halt.

As geotechnical engineering developed, Terzagihi's assumption proved to be technically and economically unfeasible. Peck (1969) proposed the inclusion of reliability methods in geotechnical engineering by use of what he called the observational method. It involves considering possible modes of unsatisfactory performance or undesirable events; developing plans for dealing with each event; making field measurements during construction to determine if the event is occurring; and modifying the design as required based on information obtained during the construction process.

Consistent with the observational method is the concept of quantifying the uncertainty. This is the purpose of reliability methods and the focus of this work. Several reliability methods are available. To discuss a few, Cornell (1969) proposed the first order second moment (FOSM) method, discussed in chapter 3

of this work, Rosenblueth (1975, 1981) proposed the point-estimate method, and with the advances in computer technology, Monte Carlo simulation can also be employed. All of which use the uncertainties in input properties to obtain a probabilistic description of the behavior of a system.

Reliability methods have been investigated for several areas of geotechnical engineering including, active earth pressure (e.g. Duncan 2000), flow through earth dams (e.g. Fenton & Griffiths 1996) and Bearing Capacity (e.g. Griffiths and Fenton 2001).

Slope stability, a geotechnical subject containing variability in soil properties and failure surfaces, has been a topic in probabilistic analysis since the 1970's (Tang et al. 1976; Matsuo and Kuroda 1974) and has continued to receive attention (e.g. Chowdhury and Tang 1987; Li and Lumb 1987; Mostyn and Li 1993; Christian et al. 1994; Wolff 1996).

The investigations use classical slope stability analysis techniques along with probabilistic methodologies. Griffiths and Fenton 2004 noted that while the investigations used sophisticated probabilistic methods, the use of a classical slope stability approach was not suitable for a highly variable soil as the shape of the failure surface was fixed. They proposed a method called the random finite element method (RFEM), discussed in chapter 4 of this work, as an analysis tool for the assessment of slope stability reliability.

Some probabilistic models characterize the uncertainty of the input parameters by assuming a mean and a standard deviation of the input parameters. Absent from this characterization of the uncertainty is the fact that geotechnical properties are also spatially correlated (e.g. Mostyn and Li 1993). For example, soil properties that are located in space close to each other tend to have similar values, while those located a significant distance apart will not have the same tendency.

Ignoring spatial correlation implies the assumption that each soil property is perfectly correlated with itself for an infinite distance. Li and White (1987) suggested that typical values of the spatial correlation length in the vertical direction were in the range of 0.1 to 5 meters and 2 to 20 meters in the horizontal direction.

The influence of including spatial correlation on the results of probabilistic methods has typically been reported to reduce the predicted probability of failure (e.g. El-Ramly et al. 2002). Thus ignoring spatial correlation was assumed to be conservative. Subsequent investigations by Griffiths and Fenton (2001) and Fenton et al. (2005), which included spatial correlation, reported a critical value for the spatial correlation length that resulted in a maximum probability of failure. The maximum probability of failure at the critical spatial correlation length was greater than the probability of failure that would have been determined if spatial correlation was ignored, suggesting that that ignoring spatial correlation length would not always lead to conservative estimates of the probability of failure.

1.3 Present Approach

The work presented in the following chapters involves the investigation of the probability of failure for a soil with spatially random shear strength parameters characterize by a mean, coefficient of variation and spatial correlation length. The geotechnical areas under investigation are a cohesionless, drained soil mass subjected to passive earth pressure and the slope stability analysis of an undrained clay. The probability of failure will be determined using the FOSM method and the RFEM and a comparison of the results will be made.

The FOSM method will assume a traditional equilibrium failure theory as the performance function in the assessment of the probability of failure. The

RFEM will incorporate random field theory with an elasto-viscoplastic finite element algorithm in a Monte Carlo framework.

The effects of interest are:

1. The influence of spatial variability on the probability of failure predicted using traditional theories and the FOSM method.
2. The influence of spatial variability on the probability of failure predicted using the RFEM.
3. A comparison of the probabilities of failure for the two methods.
4. The influence of spatial correlation on the probability of failure.

The results will give an indication of the appropriate choice for a reliability method and will give an indication of a worst-case spatial correlation which could conservatively be used in design in absence of actual soil parameter data.

2. OVERVIEW OF THE FINITE ELEMENT METHOD

2.1 Soil Model

A 2-D plane strain analysis of an elastic-perfectly plastic model as illustrated in figure 2.1 has been used in this work.

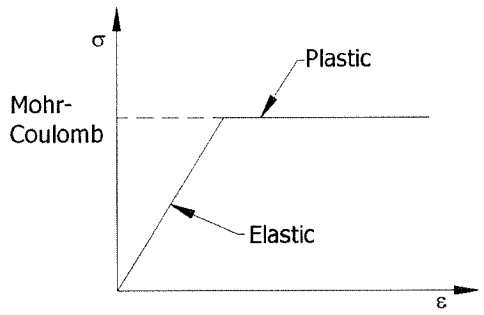


Figure 2.1: Elastic-Perfectly Plastic Soil Model

The soil model used in this study consists of the six parameters as shown in Table 2.1.

The dilation angle, ψ, controls volumetric strains during plastic yield and has little influence on collapse loads in unconfined problems such as slope stability and earth pressures (Griffiths and Lane 1999). Thus in this work, the dilation angle is assumed to be zero, corresponding to a non-associated flow rule with zero plastic volume change.

ϕ'	Friction Angle
c'	Cohesion
ψ	Dilation Angle
E	Young's Modulus
ν	Poisson's Ratio
γ	Unit Weight

Table 2.1: Six-Parameter Soil Model

The parameters c' and ϕ' refer to the effective cohesion and friction angle of the soil. The strength of the soil as an engineering material has been represented by the Mohr-Coulomb (M-C) failure criterion, the failure criterion most widely used in geotechnical practice. This criterion takes account of both the cohesive and frictional strength of a soil and contends that failure is due to a critical combination of normal and shear stress. In terms of principal stresses and assuming a sign convention where compression is negative, the criterion can be written as follows:

$$F = \frac{(\sigma'_1 - \sigma'_3)}{2}\sin\phi' - \frac{(\sigma'_1 - \sigma'_3)}{2} - c'\cos\phi' \qquad (2.1)$$

where σ'_1 and σ'_3 are the major and minor principal effective stresses at the point under consideration.

The failure function, F, is illustrated in figure 2.2 and can be interpreted as described in Table 2.2.

$F<0$	Inside M-C envelope (elastic)
$F=0$	On M-C envelope (yielding)
$F>0$	Outside M-C envelope (yielding) and stress must be redistributed

Table 2.2: Failure Function Definition

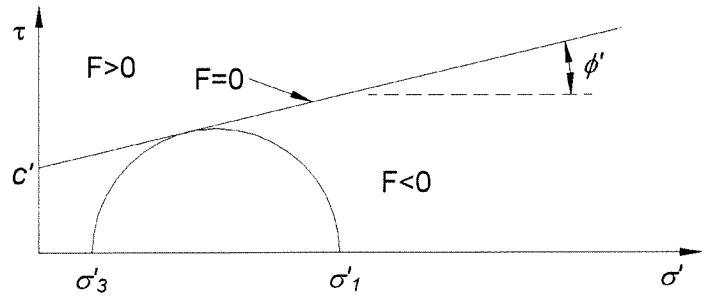


Figure 2.2: Mohr-Coulomb Failure Criterion

The elastic parameters E and ν refer to Young's modulus and Poisson's ratio of the soil. The actual values given to the elastic parameters significantly influence the computed deformations prior to failure, however they have little influence on the predicted factor of safety in slope stability or on the limiting passive force in earth pressure analysis. Thus, in this work, E and ν have been given the nominal values of $E = 10^5$ kN/m^2 and $\nu = 0.3$.

The total unit weight, γ, assigned to the soil is proportional to the nodal self-weight loads generated by gravity.

2.2 Viscoplastic Algorithm

In order to describe the behavior of a soil upon yielding and the plastic strains that then accumulate, the viscoplastic algorithm (Perzyna 1966; Zienkiewicz and Cormeau 1974), based on the 1-D rheological model shown in figure 2.3 is used.

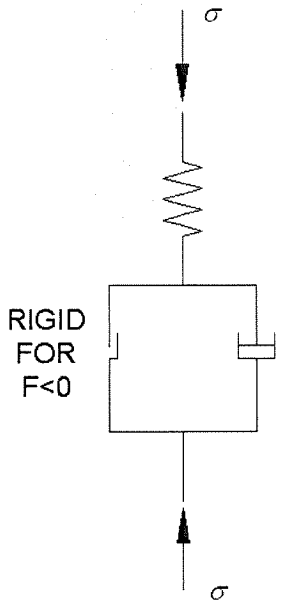


Figure 2.3: Rheological Model for 1-d Viscoplasticity

This method computes viscoplastic strains associated with stress conditions that exceed the failure criterion. The viscoplastic strains that are generated are proportional to the amount by which yield has been violated as defined by the equation:

$$\left\{\dot{\varepsilon}^{vp}\right\} = F\left\{\frac{\partial Q}{\partial \sigma}\right\} \tag{2.2}$$

where F is the value of the Mohr-Coulomb failure function (see equation 2.1), and Q is the plastic potential function. The form of equation 2.2 implies a pseudo-viscosity, which has no basis in real time and a time step is assumed to be equivalent to an iteration.

Multiplication of the viscoplastic strain rate given in equation 2.2 by a pseudo-time step gives an increment of viscoplastic strain. The strains can then be accumulated from one time step to the next by:

$$\left\{\delta\varepsilon^{vp}\right\}^{i} = \Delta t\left\{\delta\dot{\varepsilon}^{vp}\right\}^{i} \tag{2.3}$$

and

$$\left\{\Delta\varepsilon^{vp}\right\}^{i} = \left\{\Delta\varepsilon^{vp}\right\}^{i-1} + \left\{\delta\varepsilon^{vp}\right\}^{i} \tag{2.4}$$

where the superscript i refers to the time step or iteration number.

Cormeau (1975) derived a 'time step' for unconditional numerical stability for the Mohr-Coulomb failure criterion as:

$$\Delta t = \frac{4(1+\upsilon)(1-2\upsilon)}{E\left(1-2\upsilon+\sin^2\phi'\right)} \tag{2.5}$$

Stresses outside of the failure envelope are redistributed to neighboring elements that still have residual strength by accumulating them at each time-step in the body-loads vector ($\boldsymbol{F_b}$) using the integral equation given in equation 2.6.

$$\{F_b\}^i = \{F_b\}^{i-1} + \sum_{elements}^{all} \iint \left[B \right] \left[D^e \right] \left\{ \Delta \varepsilon_{vp} \right\}^i dxdy \qquad (2.6)$$

where the matrices $[B]$ and $[D]$ represent the strain-displacement and stress-strain matrices respectively.

Evaluating this integral over each element that contains a Gauss point that exceeds the failure criterion, (F>0), gives the value of the self-equilibrating forces, $\{F_b\}^i$. The force is required to be self equilibrating so that the net loading on the system is not affected. These forces are added to any actual applied external loads.

Iteration proceeds until all Gauss-point stresses have been returned to the failure surface and the convergence criterion is satisfied. Convergence is indicated when the change in the nodal displacements from one iteration to the next is less than a user defined tolerance.

Further details on the viscoplastic algorithm can be found in the text by Smith and Griffiths (2004).

2.3 Passive Earth Pressure Analysis

The soil mass is discretized into a mesh that consists of eight-node square elements. A typical finite element mesh is shown in figure 2.4.

The boundary conditions (see Figure 2.4) are such that the right side of the mesh allows vertical but not horizontal movement, the base of the mesh is fully restrained. The top and left sides of the mesh are unrestrained, with the exception of the nodes adjacent to the wall, which have fixed horizontal components of displacement. The vertical components of these displaced nodes

are free to move up, as passive conditions are mobilized, thereby modeling a perfectly smooth condition. The wall is assumed to be able to translate towards the retained soil mass a sufficient distance to mobilize the passive resistance of the soil.

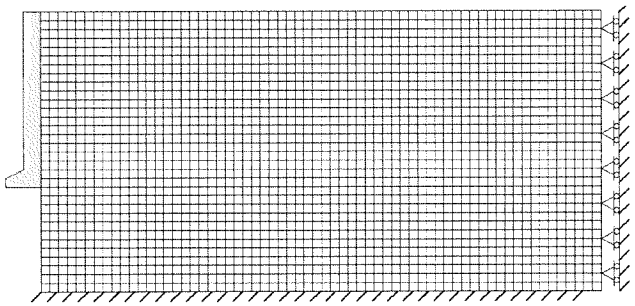


Figure 2.4: Mesh and Boundary Conditions for Passive Earth Pressure Analysis

2.3.1 Displacement Control Method

The passive wall considered is modeled by translating the nodes in contact with the wall on the upper left side of the mesh uniformly, horizontally and in the direction of the soil mass. This translation is performed incrementally, and models a rigid, smooth wall with no rotation.

The initial stress conditions in the mesh prior to translation of the nodes are that the vertical stresses equal the weight of the overburden, or

$$\sigma_v = \gamma z \tag{2.7}$$

where z is the depth to the Gauss points of the element and positive is down.

The initial horizontal stresses are defined by the coefficient of earth pressure at rest, $K_{o,}$ given by Jaky's (1944) formula in which

$$K_o = 1 - \sin\phi' \tag{2.8}$$

Following incremental displacement of the nodes, the viscoplastic algorithm monitors the stresses in all the elements (at the Gauss points) and compares them with the strength of the element based on Mohr-Coulomb's failure criterion (Griffiths 1980). If the criterion is violated, stress redistribution is initiated by the viscoplastic algorithm. The process is iterative, and convergence is achieved when all stresses within the mesh satisfy both the failure criterion and equilibrium within a user defined tolerance.

At convergence following each increment of displacement, the mobilized passive reaction force on the wall is computed by integrating the stress in the elements attached to the displaced nodes. The finite element analysis is terminated when the passive reaction force flattens out and reaches a maximum value as illustrated in figure 2.5.

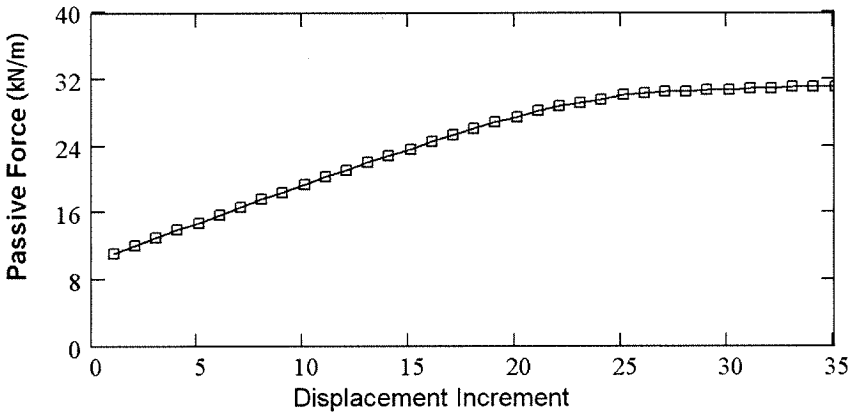


Figure 2.5: Passive Force vs. Displacement Increment

2.4 Slope Stability Analysis

The soil mass is discretized into eight node elements. For the majority of the mesh, the elements are square with equal side lengths. The elements adjacent to the slope have degenerated into triangles. The boundary conditions are such that right and left sides of the mesh allow vertical but not horizontal movement, the base of the mesh is fully restrained.

A typical finite-element mesh is shown in figure 2.6.

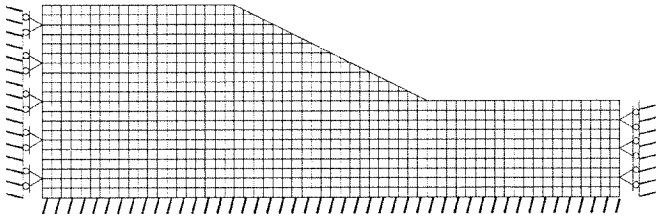


Figure 2.6: Mesh and Boundary Conditions for Slope Stability Analysis

2.4.1 Shear Strength Reduction Method

Gravity loading is applied to the slope in a single increment. The gravity load is determined by performing integration over each element of the form

$$p^{(e)} = \gamma \int_{V^e} [\mathbf{N}]^T \, d(vol) \tag{2.9}$$

where the $[N]$ terms are the shape functions of the element and the subscript e refers to the element number. The integral determines the volume of each element, multiplying this by the total unit weight of the soil gives the net vertical force per element. The net vertical force is distributed consistently to all of the nodes, assembled into a global gravity load vector and then used to generate the initial stress state of the problem. The shear and normal stresses are calculated at all Gauss points. The stresses are then compared to the failure criterion. Yielding stresses are redistributed throughout the mesh by the viscoplastic

algorithm and convergence is achieved when all stresses within the mesh satisfy both the failure criterion and equilibrium within a user defined tolerance.

Keeping the gravity load constant, the shear strength parameters are reduced by a strength reduction factor, SRF. The factored soil strength parameters that are used in the analysis are then given by equation 2.10 and 2.11.

$$\phi'_f = \tan^{-1}\left(\frac{\tan\phi'}{SRF}\right) \tag{2.10}$$

$$c'_f = \frac{c'}{SRF} \tag{2.11}$$

Several increasing values of the SRF are attempted until the algorithm fails to converge within a user defined number of iterations. It was shown by Griffiths and Fenton (2004) that an iteration ceiling greater than 200 produced consistent results. For this study, failure is said to have occurred if the algorithm was unable to converge within 500 iterations.

A more detailed description of the method is described by Griffiths and Lane (1999).

3. THE FIRST ORDER SECOND MOMENT (FOSM) METHOD

3.1 Traditional Method for a Single Random Variable

The First Order Second Moment (FOSM) is a first order approximation to the mean, μ and variance, σ^2, of a performance function, f. The performance function describes the performance of a geotechnical structure. The method is applicable for a performance function that is dependent on a number of input variables, x_i, where $i = 1,2,...,n$, that represent the soil properties. For the work considered here, a single random variable is used and the description of the method will be limited to a single variable approach. A more detail description of the method including multiple input variables can be found in the text by Baecher and Christian (2003).

The method is based on the first terms of a Taylor's series expansion of the performance function, f. The performance function could be Bishop's method of slices for slope stability analysis or Rankine's theory for earth pressure analysis. The μ_f and $\sigma^2{}_f$ of the performance function are given by equations 3.1 and 3.2.

$$\mathrm{E}[f] = \mu_f \cong f(\mu_x) \tag{3.1}$$

$$\mathrm{VAR}[f] = \sigma^2{}_f \cong \left(\frac{df}{dx}\right)^2 \sigma^2{}_x \tag{3.2}$$

where μ_x and $\sigma^2{}_x$ are the mean and variance of the input quantity, respectively. The derivative is evaluated at the mean.

For some geotechnical models, formal differentiation is too complicated and a finite difference approach can be used to approximate the derivative as follows:

$$\frac{df}{dx} \cong \frac{f\left(x^1\right) - f\left(x^2\right)}{x^1 - x^2} \tag{3.3}$$

where x^1 and x^2 represent the random variable x taken at some increment above and below the expected means. Using a small increment in equation 3.3 would more accurately estimate the value of the derivative at the expected value. Equation 3.3 is often evaluated with x^1 and x^2 taken equal to one standard deviation above and below μ_f (e.g. Duncan 2000). This collects some of the function nonlinear behavior over their most probable range (Wolff 1996), and simplifies equation 3.2 as follows:

$$\mathrm{VAR}[f] = \sigma^2{}_f \cong \left(\frac{f\left(\mu_x + \sigma_x\right) - f\left(\mu_x - \sigma_x\right)}{2} \right)^2 \tag{3.4}$$

The accuracy of the method deteriorates should second and higher order derivatives of the function be significant due to the truncation of the Taylor series after first order terms.

Another limitation of the traditional FOSM method is that spatial variability of the soil, which is the tendency for soils to vary from one location to another, is not automatically considered in the calculation of the design quantity. The

performance function is evaluated assuming a homogenous soil property, in which the value assigned to the soil property is taken based on input point statistics. The point statistics do not account for the fact that soil properties at two geotechnical sites could have identical mean and variance parameters, but one site could have properties that vary rapidly from point to point, and the other site could vary gradually.

To estimate the probability of failure, a form of the probability density function (PDF) describing the distribution of the performance function must be assumed. The most common PDF is the normal or Gaussian distribution. For a normally distributed random variable X, with a mean and standard deviation given by μ_X and σ_X, the PDF is given by equation 3.5 and illustrated in figure 3.1.

$$\mathrm{PDF}(x;\mu_X,\sigma_X) = \frac{1}{\sigma_X\sqrt{2\pi}} e^{\left\{-\frac{1}{2}\left(\frac{x-\mu_X}{\sigma_X}\right)^2\right\}} \tag{3.5}$$

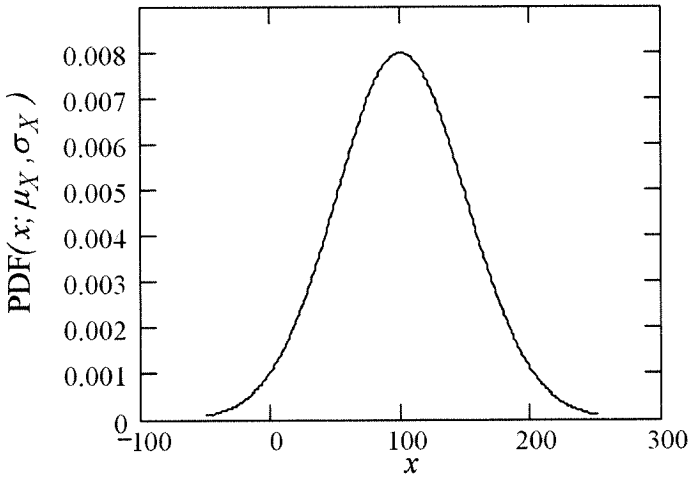


Figure 3.1: Normal PDF for $\mu_X = 100$ and $\sigma_X = 50$

The PDF describing the distribution of the performance function can also be assumed to be characterized by a lognormal distribution. A lognormally distributed random variable X, with a mean and standard deviation given by μ_X and σ_X means that $\ln X$ is normally distributed. The PDF is given by equation 3.6.

$$\text{PDF}(x;\mu_X,\sigma_X) = \frac{1}{x\sigma_{\ln X}\sqrt{2\pi}} e^{\left\{-\frac{1}{2}\left(\frac{\ln x-\mu_{\ln X}}{\sigma_{\ln X}}\right)^2\right\}} \tag{3.6}$$

where $\mu_{ln\,X}$ and $\sigma_{ln\,X}$ are the mean and standard deviation of $ln\,X$ and are given by

$$\mu_{\ln X} = \ln \mu_X - \frac{1}{2}\sigma^2_{\ln X} \tag{3.7}$$

$$\sigma_{ln\,X} = \sqrt{\ln\left\{1+\left(\frac{\sigma_X}{\mu_X}\right)^2\right\}} \tag{3.8}$$

Additional relationships that are important to the lognormal distribution are the median and the mode. The median is defined as the point where half of the area under the PDF is to the left and half is to the right. The median for a lognormal distribution is given by

$$\text{Median}_X = e^{\mu_{\ln X}} \tag{3.9}$$

The mode is defined as the most probable value and for a lognormal distribution is given by

$$\text{Mode}_X = e^{\left(\mu_{\ln X} - \sigma^2_{\ln X}\right)} \tag{3.10}$$

The lognormally distributed PDF is illustrated in figure 3.2.

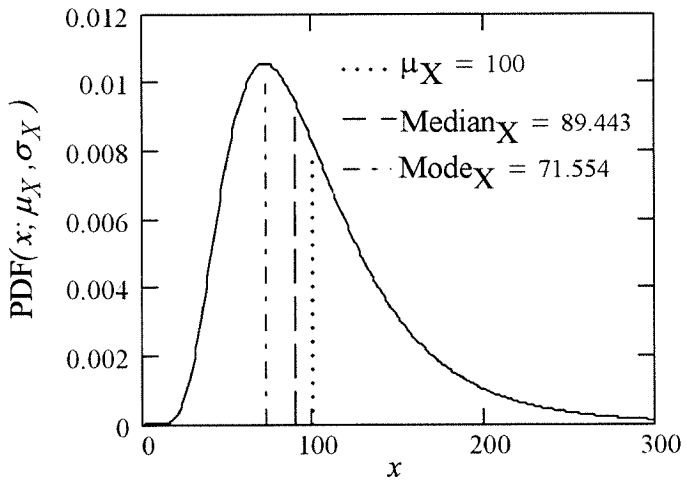


Figure 3.2: Lognormal PDF for μ_X =100 and σ_X=50

3.2 Modified Method for a Single Random Variable in 1-D

The traditional FOSM method can be modified to consider spatial variability in design by locally averaging the soil strength parameters over a predefined failure surface. The variance of the strength locally averaged over a surface is less than the variance of the point parameters.

3.2.1 Variance Reduction Over a Line

The variance reduction factor due to local averaging is defined as γ and is given by

$$\gamma = \left(\frac{\sigma^2{}_{x_A}}{\sigma^2{}_x} \right) \tag{3.11}$$

where the subscript A refers to locally averaged statistics over a line. The variance reduction factor is a function of the length over which local averaging is occurring and the correlation function. The correlation function used in this work is an exponentially decaying (Markovian) correlation function. It is the most common spatial correlation model in use (Fenton 1999a) and has the following form

$$\rho(\tau) = e^{-(2\tau/\theta)} \tag{3.12}$$

where τ is the absolute length over which local averaging is occurring, which could be an arc length for slope stability analysis or a line length for earth pressure analysis, and θ is the scale of fluctuation or the distance between two points beyond which soil properties are principally uncorrelated.

For a line of length $\tau = \alpha\theta$, shown in figure 3.3, it can be shown (Vanmarcke 1984) that the variance reduction factor is given by

$$\gamma = \frac{2}{(\alpha\theta)^2} \int_0^{\alpha\theta} e^{\left(-2\frac{x}{\theta}\right)} (\alpha\theta - x)\, dx \tag{3.13}$$

Performing the integration leads to the variance reduction values plotted in figure 3.3. Figure 3.3 illustrates that surface length impacts variance reduction. For surface lengths that are small with respect to correlation length, there is little reduction in variance, whereas surface lengths that are large relative to

correlation length can result in significant reduction which in the limit tends to zero.

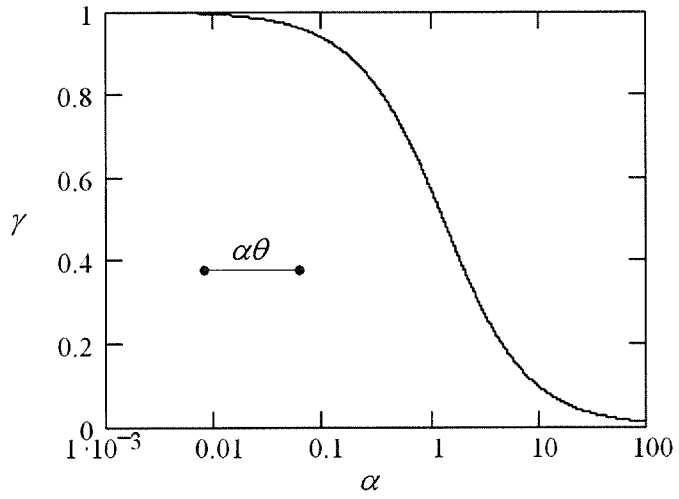


Figure 3.3: Variance Reduction Function, γ vs. α for Constant θ

The underlying statistics assuming a normal distribution and including local averaging are given by

$$\sigma_{x_A} = \sigma_x \sqrt{\gamma} \tag{3.14}$$

$$\mu_{x_A} = \mu_x \tag{3.15}$$

The performance function can be evaluated using the locally averaged statistics to determine the statistical parameters of the performance function.

It is important to note that if the point distribution of the random variable is normal, local averaging results in a reduced standard deviation but the mean is

unaffected. If the point distribution is lognormal, both the mean and the standard deviation are reduced by local averaging. This is due to the fact that the mean of a lognormal relationship depends on both the mean and the variance of the underlying normal relationship (see Equations 3.16 and 3.17).

$$\mu_x = e^{\left(\mu_{\ln x} + \frac{1}{2}\sigma^2_{\ln x}\right)} \tag{3.16}$$

$$\sigma_x = \mu_x \sqrt{e^{\left(\sigma^2_{\ln x}\right)} - 1} \tag{3.17}$$

4. THE RANDOM FINITE ELEMENT METHOD (RFEM)

The random finite element method (RFEM), first described Fenton and Griffiths (1993), combines elastoplastic finite element analysis with random field theory and is a powerful general method of accounting for spatially random soil properties and spatial correlation. In this method, a random field of soil properties is generated using the Local Average Subdivision (LAS) method (Fenton and Vanmarcke 1990; Fenton 1999b) and mapped onto a finite element mesh.

4.1 Characterization of the Input Random Variable

The soil property considered to be a random variable is assumed to be characterized by a lognormal distribution and having input parameters of a mean, μ_x, a standard deviation, σ_x, and a spatial correlation length, $\theta_{\ln x}$. The μ_x and σ_x can be expressed in terms of the dimensionless coefficient of variation, V, defined as

$$V_x = \frac{\sigma_x}{\mu_x} \tag{4.1}$$

The $\theta_{\ln x}$ can be normalized by a geometric property of the analysis considered and can be expressed in the dimensionless form,

$$\Theta_{\ln x} = \frac{\theta_{\ln x}}{H} \tag{4.2}$$

where H, for example, is the embankment height for a slope stability analysis.

Use of a lognormal distribution to characterize the input soil properties is preferred over the normal distribution because it avoids the generation of negative values. Additionally, available field data indicate a lognormal distribution for some soil properties (Hoeksema and Kitanidid 1985; Sudicky 1986; Cherubini 2000).

4.2 Variance Reduction of Input Parameters

To account for the fact that the input parameters are defined at a point level, local averaging is performed over the size of the element and the variance reduction factor, γ (see equation 3.11), is used to adjust the point statistics used in the elastoplastic finite element analysis.

The variance reduction factor, γ, is a function of element size and the correlation function. It is assumed that the soil is isotropic, which means that the spatial correlation lengths in the vertical and the horizontal direction are assumed to be equal. The correlation function used in this work is an exponentially decaying (Markovian) correlation function represented in the form

$$\rho(\tau) = e^{-\left(\frac{2}{\theta_{\ln x}}\sqrt{\tau_x{}^2 + \tau_y{}^2}\right)} \tag{4.3}$$

where τ_x is the difference between the x coordinates of any two points in the random field; and τ_y is the difference between the y coordinates.

For a square finite element of side length $\alpha\theta_{\ln x}$ it can be shown (Vanmarcke 1984) that γ is given by

$$\gamma = \frac{4}{\left(\alpha\theta_{\ln x}\right)^4} \int_0^{\alpha\theta_{\ln x}} \int_0^{\alpha\theta_{\ln x}} e^{\left(\frac{-2}{\alpha\theta_{\ln x}}\sqrt{\tau_x^2+\tau_y^2}\right)} \left(\alpha\theta_{\ln x}-\tau_x\right)\left(\alpha\theta_{\ln x}-\tau_y\right) dxdy \qquad (4.4)$$

Performing the integration leads to the variance reduction values plotted in figure 4.1.

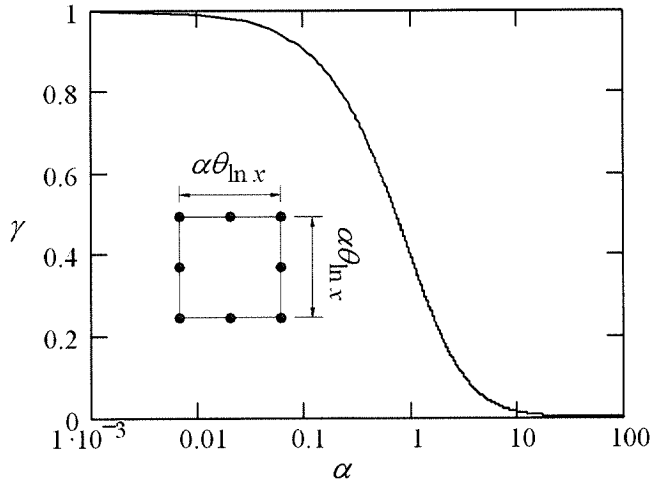


Figure 4.1: Variance Reduction Function, γ vs. α for Constant $\theta_{\ln x}$

The results for a square element can be interpreted as elements that are small relative to correlation length lead to little reduction in variance, whereas elements that are large relative to correlation length lead to significant variance reduction.

The statistics of the underlying log field, including local averaging, are therefore given by

$$\sigma_{\ln x_A} = \sigma_{\ln x}\sqrt{\gamma} \tag{4.5}$$

$$\mu_{\ln x_A} = \mu_{\ln x} \tag{4.6}$$

This leads to the following statistics of the lognormal field, including local averaging, that is actually mapped onto the finite element mesh from equations 3.16 and 3.17, thus

$$\mu_{x_A} = e^{\left(\mu_{\ln x_A} + \frac{1}{2}\sigma^2_{\ln x_A}\right)} \tag{4.7}$$

$$\sigma_{x_A} = \mu_{x_A}\sqrt{e^{\left(\sigma^2_{\ln x_A}\right)} - 1} \tag{4.8}$$

4.3 Simulation Via Local Average Subdivision

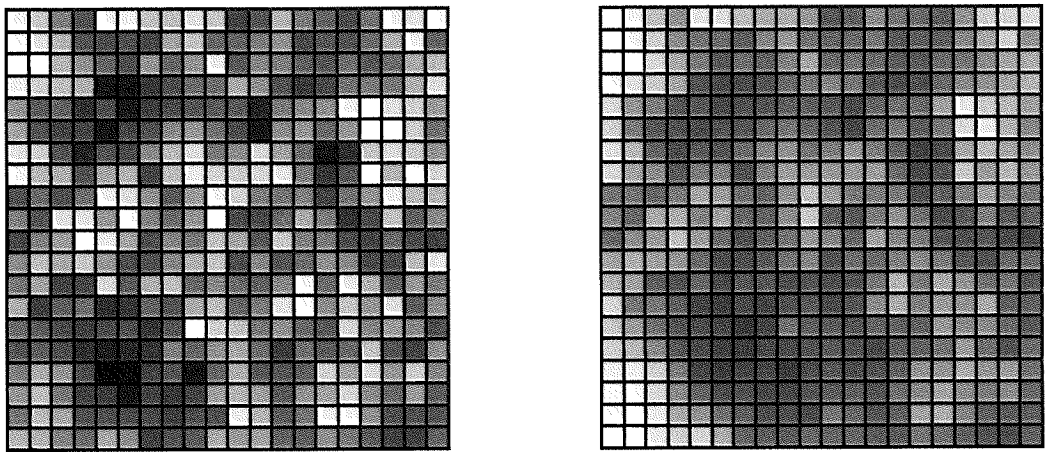
A lognormally distributed random field is obtained by first simulating a normally distributed random field, $G(\tau)$, where τ is the location in 2-D space and $G(\tau)$ is the local average of a normally distributed field governed by the correlation function given in equation 4.3. The simulated random field has a zero mean, a unit variance, and a spatial correlation length, $\theta_{\ln x}$. The underlying normally distributed random field is transformed to the desired soil property field using the relationship

$$x_i = e^{\left(\ln \mu_x + \sigma_{\ln x} G\left(\underset{\sim}{x}_i\right)\right)} \tag{4.9}$$

where $\underset{\sim}{x}_i$ is a vector containing the coordinates of the center of the i^{th} element and x_i is the random soil value assigned to that element.

In the RFEM, the value assigned to each element is constant and is itself a random variable. The element random variables are correlated to one another by the spatial correlation length.

The influence of spatial correlation length on the mapped random soil values is illustrated in figure 4.2 in the form of grey scale in which weaker regions are lighter and stronger regions are darker. An example of relatively low spatial correlation length and a relatively high correlation length are shown. The mean and the standard deviation of the random variable being mapped to the mesh are the same in both figures.



Low correlation length High correlation length

Figure 4.2: Typical Random Fields in the RFEM Method

4.4 Monte Carlo Simulation

For each set of assumed statistical properties given by μ_x, V_x and $\Theta_{\ln x}$, Monte Carlo simulations are performed. These involve the generation of a random field and the subsequent finite element analysis for each simulation, also referred to as a realization. Each realization, while having the same underlying input statistics, will have a different spatial pattern for the soil property being mapped to the mesh. In other words, the location of the stronger and weaker elements in the mesh will vary from realization to realization. An example of this is illustrated in figure 4.3.

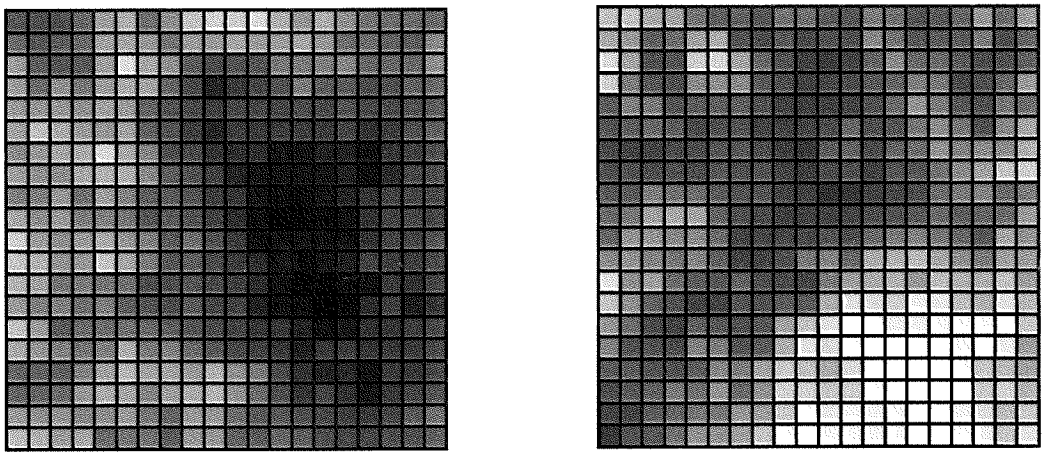


Figure 4.3: Typical random fields in the RFEM method for constant statistical input parameters μ_x, V_x and $\Theta_{\ln x}$

Each realization will therefore have a distinctive finite element result. On completing a set number of realizations, the finite element results are then subjected to a statistical analysis.

4.4.1 Influence of the Number of Monte Carlo Simulations

The accuracy of the estimated finite element statistics depends on the number of realizations carried out for each set of input parameters. Enough realizations must be analyzed so that the calculated statistics are stable or reproducible. The influence of the number of realizations on the mean and standard deviation of the passive force on a wall is shown in figure 4.4.

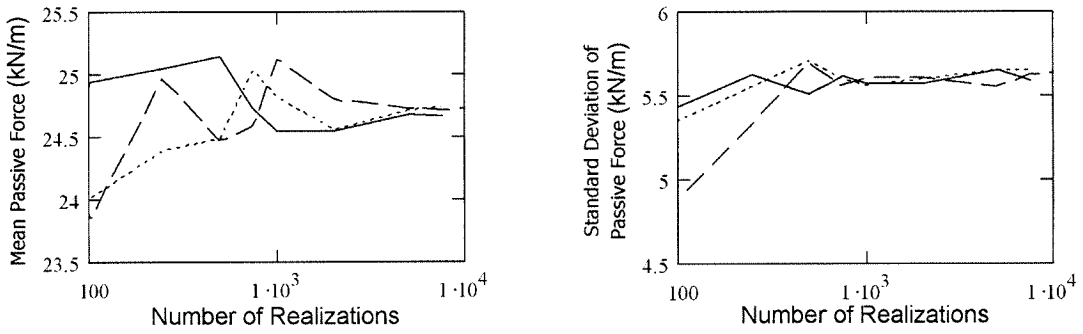


Figure 4.4: Effect of the Number of Realizations on the Passive Force Statistics

It can be observed that 1000 realizations is generally adequate for the passive earth case and therefore used in this work. It has been determined (Griffiths and Fenton 2004) that 1000 realizations was also adequate for the slope stability analysis and is used in this work.

The standard error associated with the statistics produced by the RFEM is a function of the magnitude of the probability of failure and the number of realizations. It is given by

$$\sigma_{p_f} = \sqrt{\frac{p_f\left(1-p_f\right)}{n}} \tag{4.10}$$

where n is the number of realizations and p_f is the estimated probability of failure. The results of evaluating equation 4.10 with n=1000 are shown in figure 4.5. From figure 4.5, the standard error is about 0.01 when p_f= 0.20 and 0.005 when p_f= 0.05.

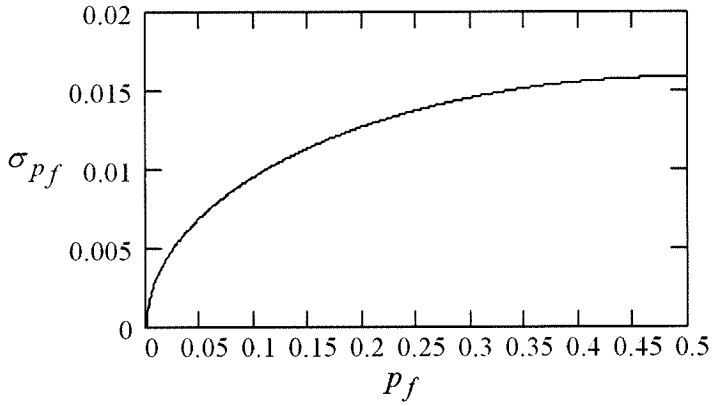


Figure 4.5: Standard error versus probability of failure for 1000 Monte Carlo Realizations

5. PASSIVE EARTH PRESSURE

The specific case of a two-dimensional cohesionless drained soil mass with a horizontal upper surface retained by a vertical, frictionless, rigid wall is examined. For the cohesionless soil considered, the soil properties of interest are the friction angle, ϕ', and the unit weight, γ.

The friction angle is assumed to be a spatially random variable, characterized by a mean, standard deviation and correlation length. The friction angle is assumed to vary between 0° and 90° so that a lognormal distribution would not be appropriate. However, $\tan \phi'$ varies between 0 and infinity and thus an appropriate distribution could be the lognormal, therefore a lognormal distribution of $\tan \phi'$ is considered in this work. The mean and standard deviation are expressed in terms of the dimensionless coefficient of variation, defined as

$$V_{\tan\phi'} = \frac{\sigma_{\tan\phi'}}{\mu_{\tan\phi'}} \tag{5.1}$$

The spatial correlation normalized by the wall height is

$$\Theta_{\ln \tan\phi'} = \frac{\theta_{\ln \tan\phi'}}{H} \tag{5.2}$$

where H is the height of the wall is shown in figure 5.1 and taken to be a unit length.

The range of parameters considered for $\tan \phi'$ are based on the work of Lumb (1966), Lacasse and Nadim (1996) and Phoon and Kulhawy (1999). The values considered are shown in table 5.1.

Parameter	Values Considered
$V_{\tan \phi'}$	0.02, 0.05, 0.1, 0.2, 0.3, 0.5
$\Theta_{\ln \tan \phi'}$	0.025, 0.05, 0.1, 0.2, 0.5, 1.0, 2.0, 5.0

Table 5.1: Parameters varied in study

A mean value of $\mu_{\tan \phi'} = 0.57735$, which corresponds to a value of $\mu_{\phi'} = 30^{o}$, will be used.

The unit weight of the soil is not considered to be a random variable because the variability is small relative to the friction angle. The unit weight is assumed to be 20. Units are not used herein as the results are applicable to any consistent set of length and force units.

5.1 Rankine Theory of Earth Pressure

The traditional theory of lateral passive earth pressures against a smooth wall is derived from equations of equilibrium along an assumed planar failure surface passing through the soil mass as illustrated in Figure 5.1.

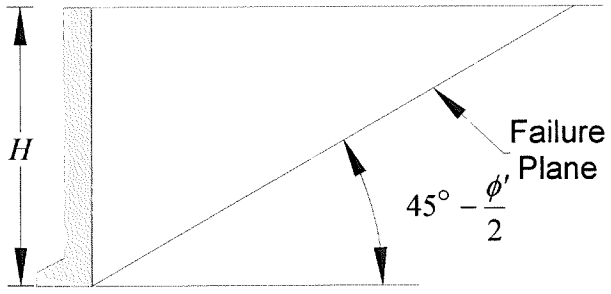


Figure 5.1: Traditional failure plane

For cohesionless soil, c'=0, and a constant friction angle Rankine's theory of earth pressure gives the passive earth pressure coefficient to be

$$K_p = \tan^2\left(45 + \frac{\phi'}{2}\right) \tag{5.3}$$

Written in terms of $\tan\phi'$ yields

$$K_p = \left[\tan\phi' + \sqrt{1 + \tan^2\phi'}\right]^2 \tag{5.4}$$

The soil's drained friction angle is ϕ'.

The total lateral passive earth force acting on a smooth wall of height H, at height $H/3$, is given by equation 5.5.

$$P_p = \frac{1}{2}\gamma H^2 K_p \tag{5.5}$$

5.2 First Order Second Moment (FOSM) Method

The FOSM method will be performed assuming the performance function defined by equation 5.5. Therefore, the mean value of the passive earth resistance P_p, using equation 3.1, is defined by

$$\mathrm{E}[P_p] = \mu_{P_p} \cong \frac{1}{2}\gamma H^2 \left[\mu_{\tan\phi'} + \sqrt{1 + \mu_{\tan\phi'}^{\,2}} \right]^2 \tag{5.6}$$

The variance, using equation 3.2, is defined by

$$\mathrm{VAR}[P_p] = \sigma^2{}_{P_p} \cong \left(\frac{2\left[\mu_{\tan\phi'} + \sqrt{1 + \mu_{\tan\phi'}^{\,2}} \right]^2}{\sqrt{1 + \mu_{\tan\phi'}^{\,2}}} \right)^2 \sigma^2{}_{\tan\phi'} \tag{5.7}$$

The modified method that accounts for spatial correlation will be used, therefore the values used in equations 5.6 and 5.7 will be adjusted due to local averaging. The failure surface over which local averaging will be performed is assumed to be that defined by

$$S = \frac{H}{\sin\left(45^\circ - \frac{\phi'}{2}\right)} \tag{5.8}$$

where ϕ' is taken to be $\mu_{\phi'} = 30^{o}$ and H is the height of the wall.

The failure surface will be subdivided into equal sections and local averaging will be performed over the subdivided lengths. The local average length will be represented as $\alpha\theta$ (see Figure 3.3)

The relationship between the number of subdivisions and $\alpha\theta$, normalized with respect to the wall height is illustrated in figure 5.2.

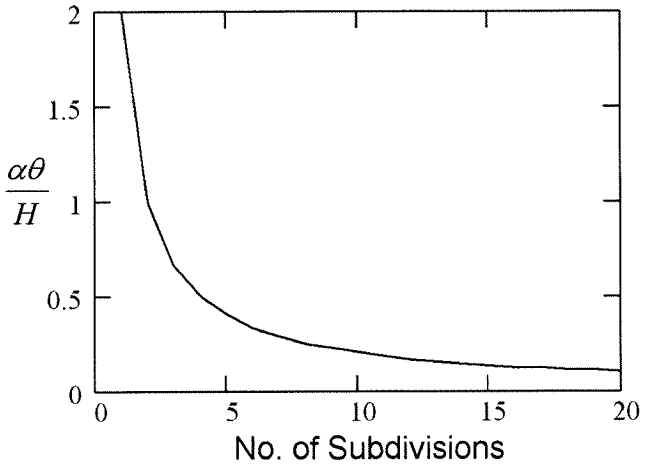


Figure 5.2: $\frac{\alpha\theta}{H}$ vs. Number of Subdivisions

5.2.1 Variance Reduction due to Local Averaging

The influence of the number of subdivisions on the locally averaged statistics, normalized by the input statistics, is illustrated in figure 5.3.

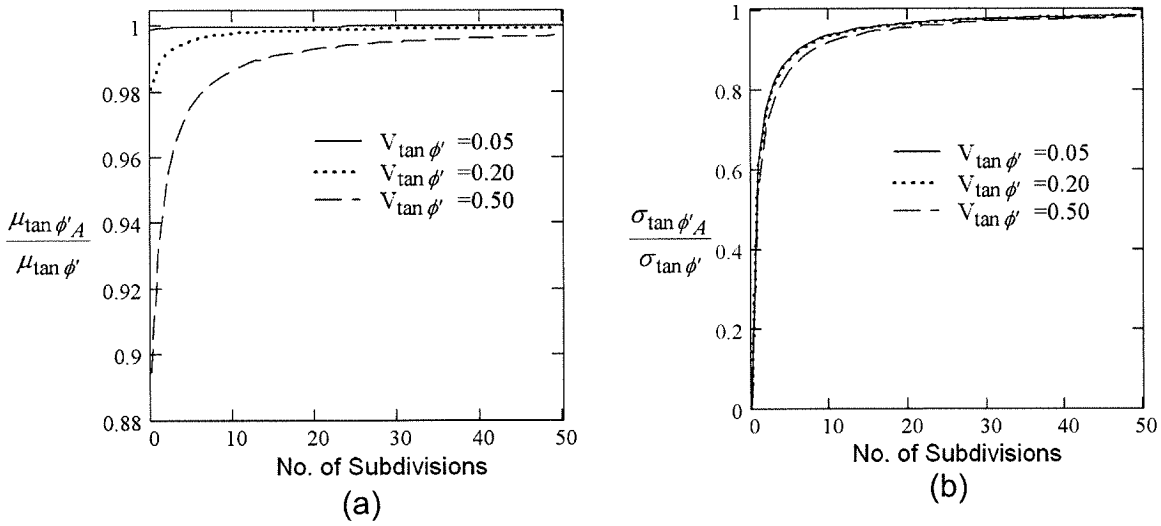


Figure 5.3: Influence of number of subdivisions on local averaging: influence on the (a) mean and (b) standard deviation for $\Theta_{\ln\tan\phi'} = 1.0$

Figure 5.3 illustrates that for larger numbers of subdivisions, the locally averaged statistics approach the input statistics. A large number of subdivisions indicate that the line length is small with respect to the spatial correlation length and the locally averaged statistics closely resemble the input point statistics. Conversely, for a fewer number of subdivisions, the line lengths are large with respect to the spatial correlation length and the locally averaged statistics are reduced with respect to the input statistics. As the number of subdivisions tends to zero, the locally averaged mean approaches the median value (see Equation 3.9) of the input statistics and the standard deviation tends toward zero.

5.2.2 Design Reliability

The reliability of the design depends on the relationship between the predicted and actual lateral loads. Defining the design wall resistance, R as

$$R = \frac{P_p}{FOS} \tag{5.9}$$

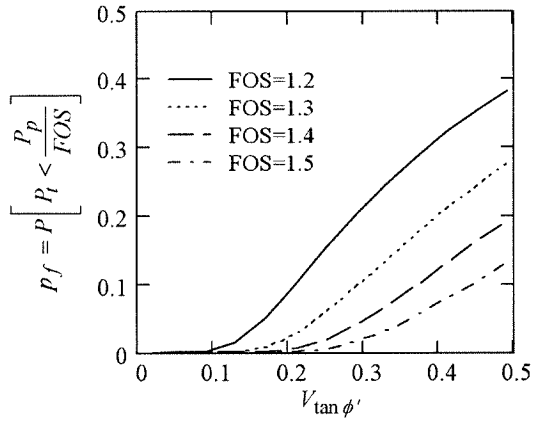
where FOS is a factor of safety and P_p is the predicted passive lateral earth load, then the wall will not fail if the true passive lateral resistance is greater than $\frac{P_p}{FOS}$ assuming the design purpose of the wall is an anchorage system. The probability of failure of the retaining system will be defined as the probability that the true lateral load, P_t, is less than the factored resistance:

$$p_f = P[P_t < R] = P\left[P_t < \frac{P_p}{FOS}\right] \tag{5.10}$$

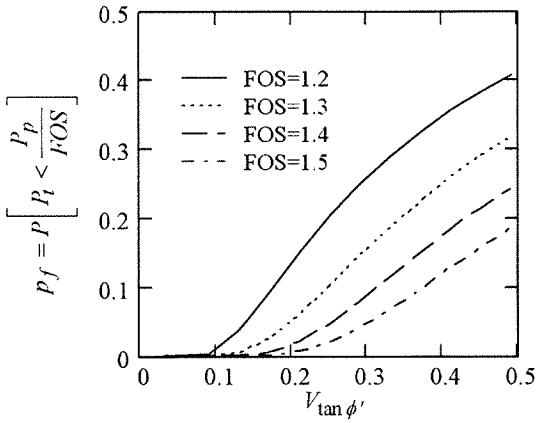
where P_t is assumed to be the load computed using equation 5.5 with $\phi' = \mu_{\phi'}$ and the form of the probability density function is assumed to be lognormal.

5.2.3 FOSM Method Results

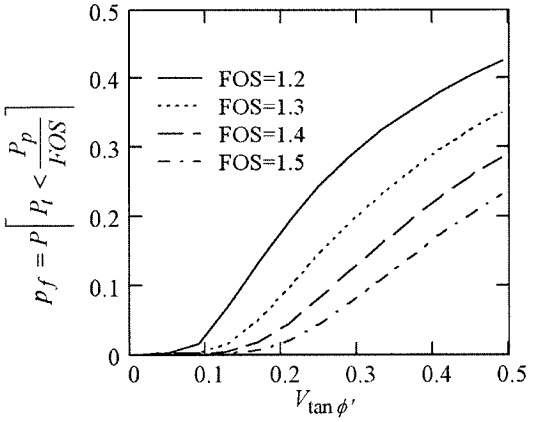
Figure 5.4 illustrates the influence of $V_{\tan\phi'}$ and the number of subdivisions on the estimated probability of failure.



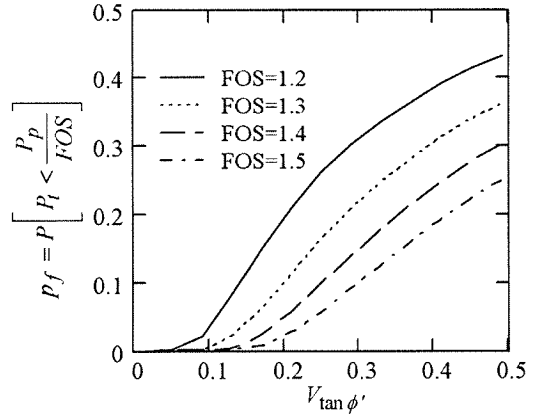
(a) Number of Subdivisions = 1



(b) Number of Subdivisions = 2



(c) Number of Subdivisions = 6



(d) Number of Subdivisions = 20

Figure 5.4: Estimated probability of failure, p_f, that the true lateral passive load will be less than the factored predicted design load for $\Theta_{\ln\tan\phi'} = 1.0$.

Figure 5.4 indicates that the estimated probability of failure increases as the number of subdivisions increases and as the soil becomes increasingly variable. Additionally the estimated probability of failure decreases as the number of subdivisions decreases. This is more clearly shown in figure 5.5. A fewer number of subdivisions indicates a longer length over which local averaging is taking place and the greater the influence of local averaging in the form of a reduced mean and standard deviation (see figure 5.3).

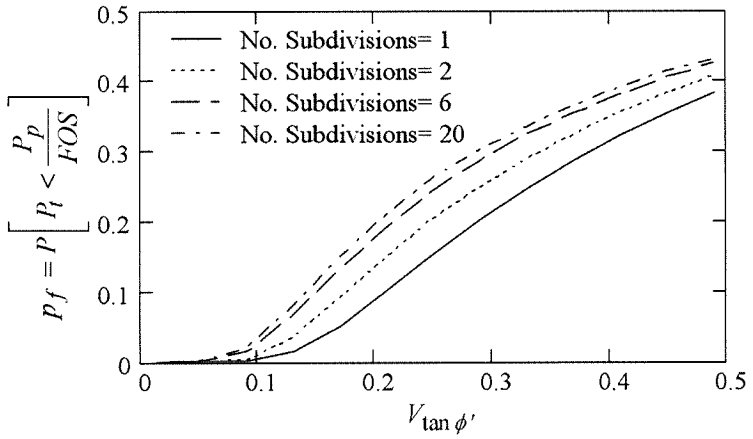
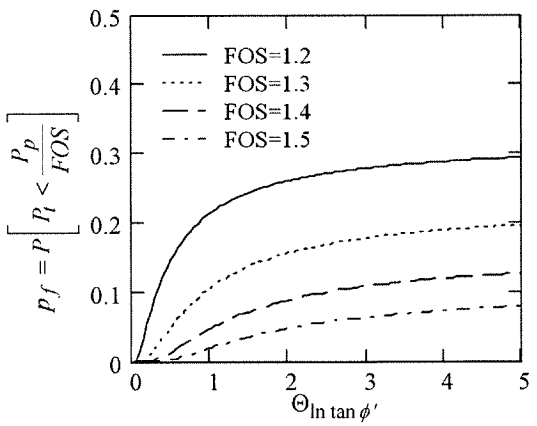
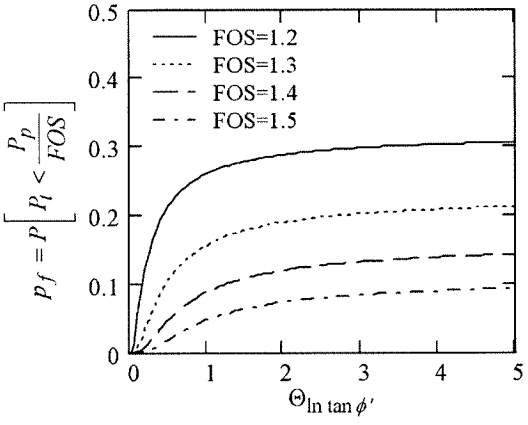


Figure 5.5: Estimated probability of failure, p_f, that the true lateral passive load will be less than the factored predicted design load for $\Theta_{\ln\tan\phi'} = 1.0$ and *FOS=1.2.*

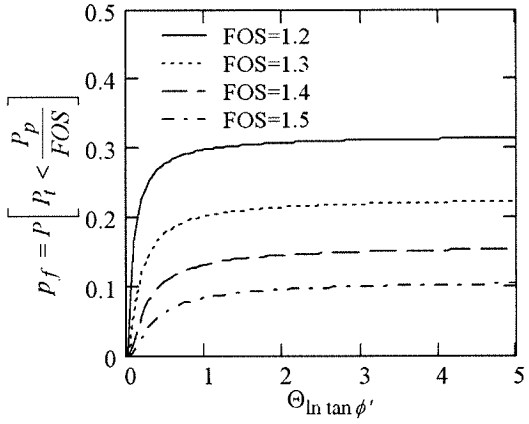
Figure 5.6 illustrates the influence of $\Theta_{\ln\tan\phi'}$ and the number of subdivisions on the estimated probability of failure.



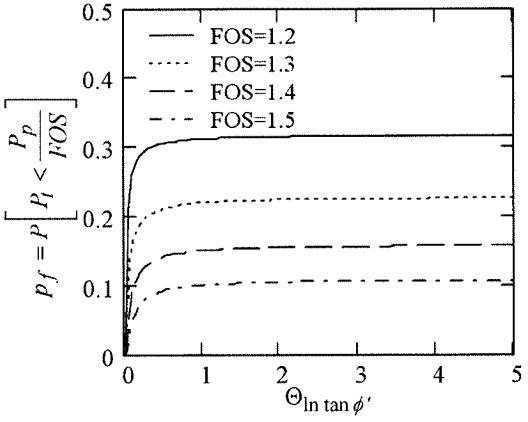
(a) Number of Subdivisions = 1



(b) Number of Subdivisions = 2



(c) Number of Subdivisions = 6



(d) Number of Subdivisions = 20

Figure 5.6: Estimated probability of failure, p_f, that the true lateral passive load will be less than the factored predicted design load for $V_{\tan \phi'} = 0.30$.

From figure 5.6, it can be observed that the probability of failure reaches a maximum value as the correlation length increases. The maximum value is that which would be obtained assuming no local averaging, which implies a spatially uniform soil or a spatial correlation length equal to infinity. The estimated probability of failure assuming $\Theta_{\ln \tan \phi'} = \infty$ is shown in figure 5.7 with the values for $V_{\tan \phi'} = 0.30$ represented to allow comparison to figure 5.6.

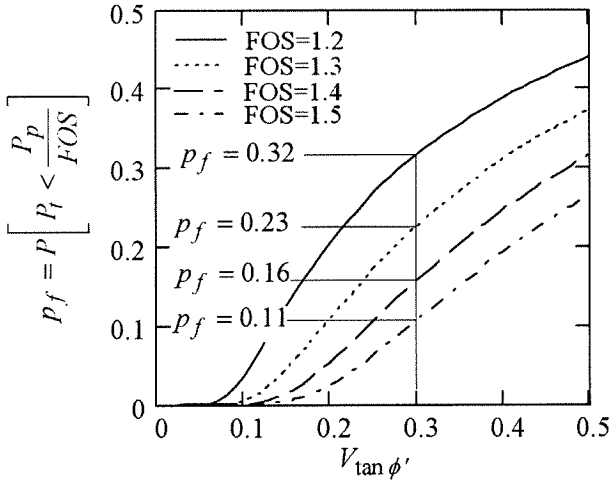


Figure 5.7: Estimated probability of failure, p_f, that the true lateral passive load will be less than the factored predicted design load for $V_{\tan \phi'} = 0.30$ and $\Theta_{\ln \tan \phi'} = \infty$.

The influence of the number of subdivisions on the estimated probability of failure is illustrated in figure 5.8.

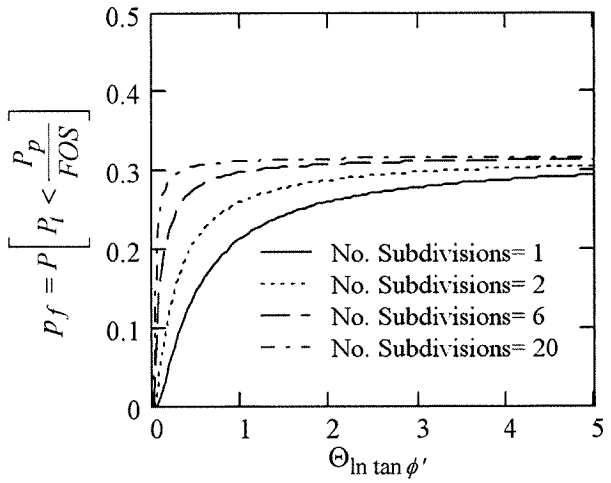


Figure 5.8: Estimated probability of failure, p_f, that the true lateral passive load will be less than the factored predicted design load for $V_{\tan \phi'} = 0.30$ and $FOS=1.2$.

The estimated probability of failure increases as the number of subdivisions increases. This is in agreement with the results from figure 5.3 which indicate that as the number of subdivisions increases the locally averaged statistics closely resemble the input point statistics which result in a maximum value for the estimated probability of failure.

5.3 Random Finite Element Method

The soil mass is discretized into a mesh that consists of 64 eight-node plane strain square elements in the horizontal direction by 32 elements in the vertical direction as shown in figure 2.4. Each element has a side length of 0.05,

recalling that units are not used herein as the results are applicable to any consistent set of length and force units. The wall extends to a depth of 20 elements or a unit length along the left face.

The study will assume that $\tan \phi'$ is a log-normally distributed field: hence K_o (see Equation 2.8) will be a random field dependent on ϕ' and the horizontal initial stresses will vary randomly down the face of the wall.

The finite element model used in this study includes the soil dilation angle, taken to be zero, Poisson's ratio, taken to be 0.3 and Young's modulus, taken to be 10^5. As stated before, the unit weight is taken to be 20. These properties are assumed to be spatially constant.

5.3.1 Design Reliability

The wall resistance, R, is as defined by equation 5.9. The probability of failure is as defined by equation 5.10. In the RFEM, the true lateral load, $P_{t,}$ is assumed to be the load computed in the finite element analysis for each soil realization.

The predicted lateral load, $P_{p,}$ depends on an estimate of the friction angle, ϕ'. In this work, the friction angle will be estimated using a 'virtual sample' and the predicted lateral load based on virtual sampling will be represented by $P_{p_{VS}}$.

The phrase 'virtual sample' means that the friction angle is sampled from the finite element mesh for each realization. If $\underset{0}{\tau}_S$ is the coordinates of the sample point, the friction angle is obtained from each random field realization as

$$\hat{\phi}' = \tan^{-1}\left\{\tan\left[\phi'\left(\underset{0}{\tau}_S\right)\right]\right\} \tag{5.11}$$

The predicted virtually sampled lateral load, $P_{p_{vs}}$, is then defined as

$$P_{p_{vs}} = \frac{1}{2}\gamma H^2 \tan^2\left(45 + \frac{\hat{\phi}'}{2}\right) \tag{5.12}$$

The probability of failure is then defined as the proportion of the number simulations that results in $P_{p_{vs}}$ being less than the factored true lateral load.

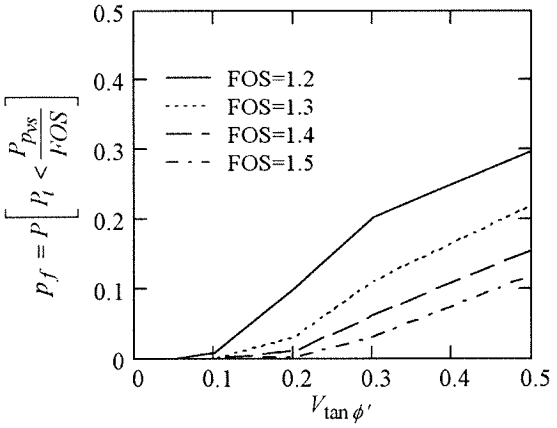
Table 5.2 lists the location of the sample points used in this study.

Virtual Sample Point No.	Horizontal distance from base of wall	Vertical distance from soil surface
1	$H/4$	$H/2$
2	$H/2$	$H/2$
3	H	$H/2$
4	$2H$	$H/2$

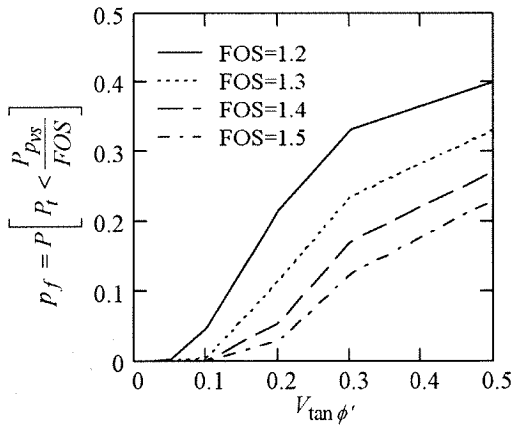
Table 5.2: Location of virtual sample points in study

5.3.2 Monte Carlo Results Based on Virtual Sampling

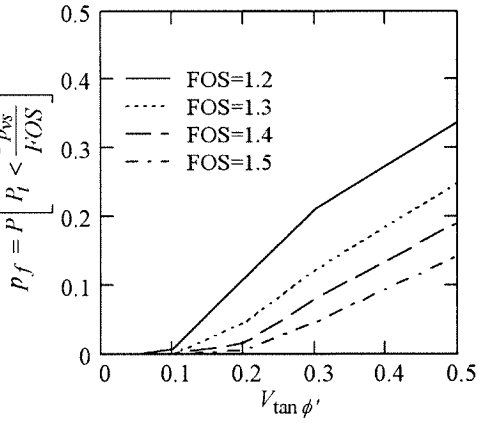
Figure 5.9 illustrates the influence of $V_{\tan\phi'}$ and $\Theta_{\ln\tan\phi'}$ on the estimated probability of failure, p_f, for a single virtual sample located as described for virtual sample point 1.



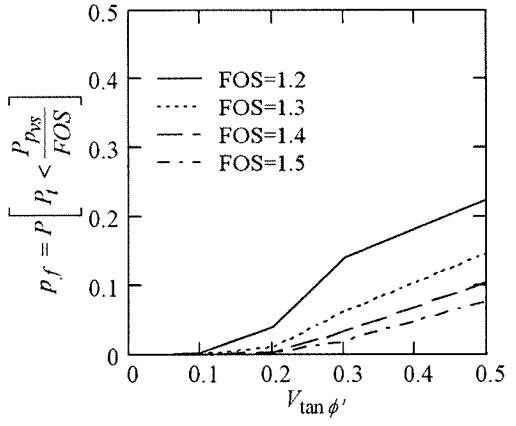
(a) $\Theta_{\ln\tan\phi'} = 0.05$



(b) $\Theta_{\ln\tan\phi'} = 0.2$



(c) $\Theta_{\ln\tan\phi'} = 2.0$



(d) $\Theta_{\ln\tan\phi'} = 5.0$

Figure 5.9: Estimated probability of failure, p_f, that the true lateral passive load will be less than the factored predicted design load for virtual sample point 1 for (a) $\Theta_{\ln\tan\phi'} = 0.05$, (b) $\Theta_{\ln\tan\phi'} = 0.2$, (c) $\Theta_{\ln\tan\phi'} = 2.0$, and (d) $\Theta_{\ln\tan\phi'} = 5.0$.

From figure 5.9 illustrates that as the soil becomes more variable, the probability of failure once again increases. The impact of varying the spatial correlation length can be better illustrated by figure 5.10.

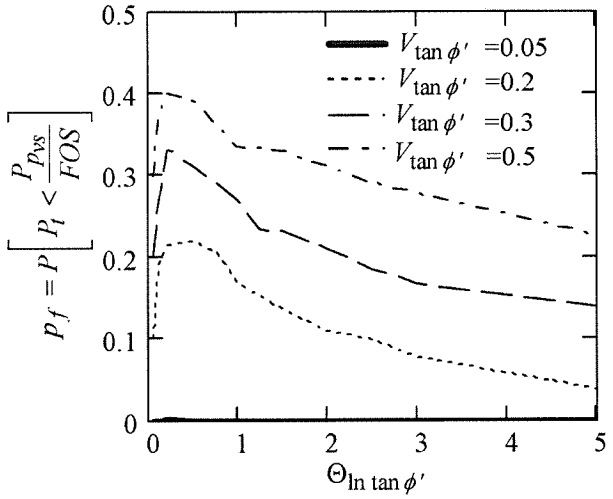
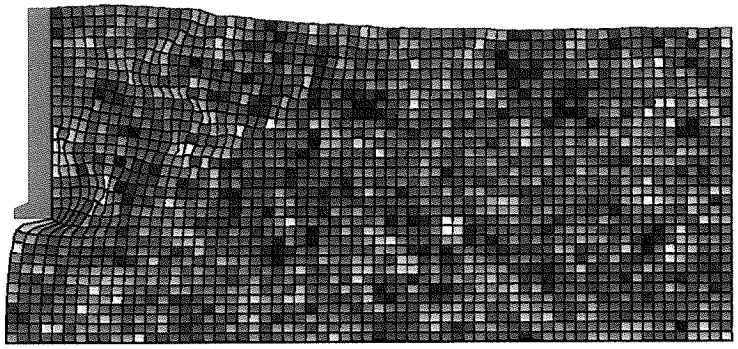


Figure 5.10: Estimated probability of failure, p_f, that the true lateral passive load will be less than the factored predicted design load for $FOS=1.2$.

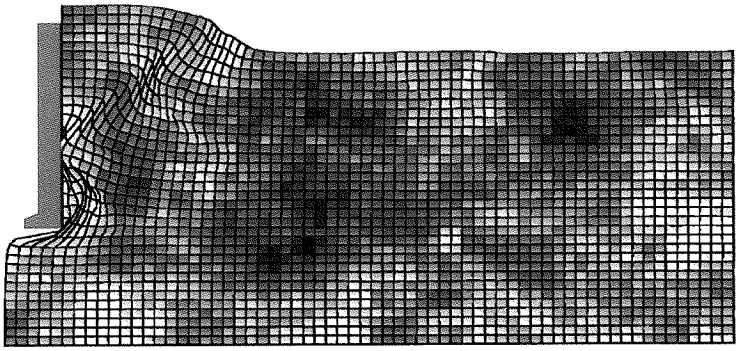
Figure 5.10 illustrates that there is a critical value of $\Theta_{\ln\tan\phi'}$ that leads to the maximum estimated probability of failure. The identification of a critical value of spatial correlation length is consistent with a number of classical geotechnical problems that were evaluated using the RFEM. This result was identified for bearing capacity and active earth pressure by Fenton and Griffiths (2001) and Fenton et al. (2005), respectively.

For values of $\Theta_{\ln \tan \phi'}$ near the critical value, the soil spatial variability is such that a single virtual sample is not sufficient to characterize the soil mass and traditional theories fail to accurately predict the passive force. Additionally, the soil mass modeled by the RFEM for intermediate values of $\Theta_{\ln \tan \phi'}$ allows for weak zones to be created in the random finite element mesh (see figure 5.11).

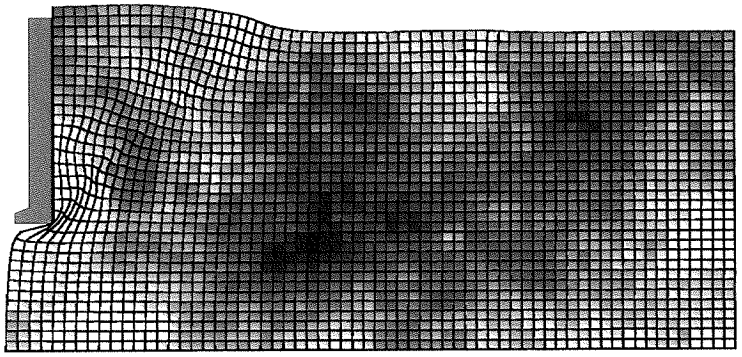
The failure surface forms at regions of a lower friction angle or weak zones, and follows a path not defined by traditional theory but characterized by regions of lower strength. To better illustrate the failure mechanism, the plastic shear strain invariant has been contoured at failure (see figure 5.12) for the soil realizations shown in figure 5.11. The Rankine failure plane has been drawn onto the contour as a black line to better illustrate the difference between the assumed failure surface and the actual failure surface for the soil realization. Large values of the shear strain invariant are indicated by darker regions and lighter regions indicate smaller values.



(a) $\Theta_{\ln \tan \phi'} = 0.05$

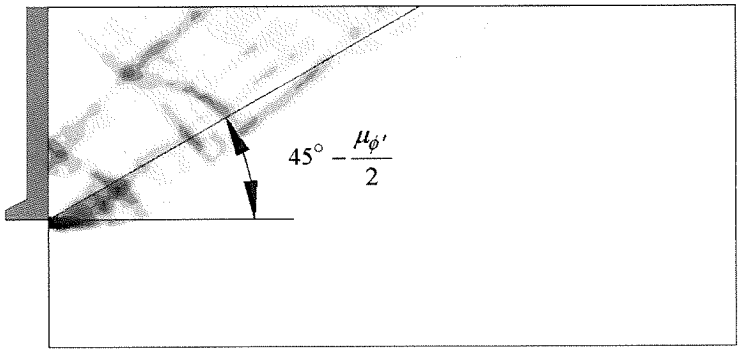


(b) $\Theta_{\ln \tan \phi'} = 0.5$

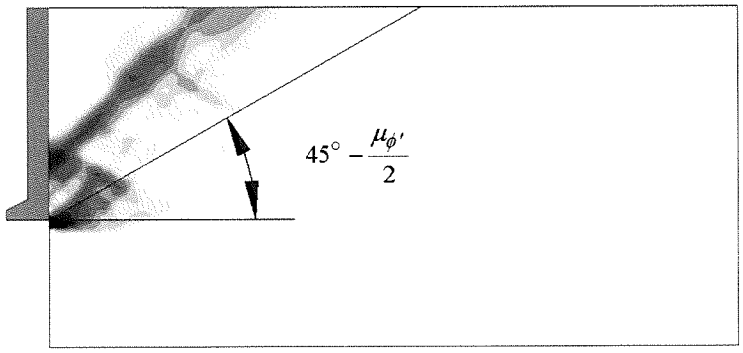


(c) $\Theta_{\ln \tan \phi'} = 5.0$

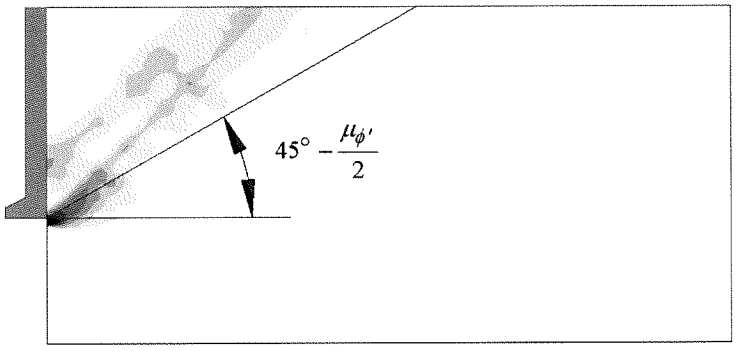
Figure 5.11: Passive earth displacement for a soil friction angle realization, $V_{\tan \phi'} = 0.5$ and
(a) $\Theta_{\ln \tan \phi'} = 0.05$, (b) $\Theta_{\ln \tan \phi'} = 0.5$, and (c) $\Theta_{\ln \tan \phi'} = 5.0$.



(a) $\Theta_{\ln \tan \phi'} = 0.05$



(b) $\Theta_{\ln \tan \phi'} = 0.5$



(c) $\Theta_{\ln \tan \phi'} = 5.0$

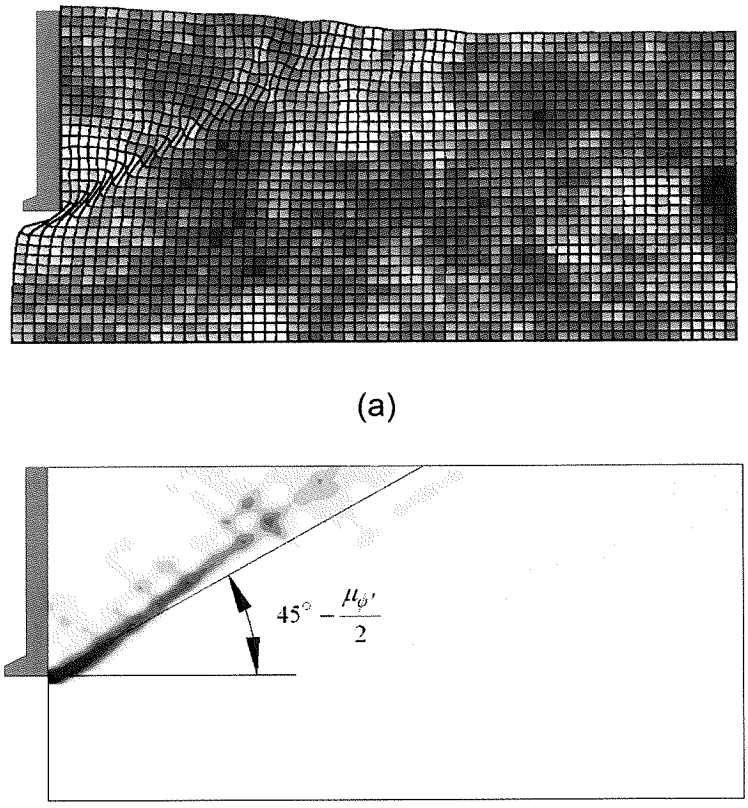
Figure 5.12: Contour of shear strain invariant for soil friction angle realization illustrated in figure 5.11 for
(a) $\Theta_{\ln \tan \phi'} = 0.05$, (b) $\Theta_{\ln \tan \phi'} = 0.5$, and (c) $\Theta_{\ln \tan \phi'} = 5.0$.

Figure 5.12b illustrates that the failure surface does not coincide with the Rankine failure surface evaluated at the mean for the intermediate value of $\Theta_{\ln \tan \phi'} = 0.5$. Locations of strong zones of soil near the wall have influenced the failure mechanism to 'seek out' a path not characterized by traditional theory.

For large values of $\Theta_{\ln \tan \phi'}$ the soil properties do not vary rapidly from point to point (see Figure 5.11c). The virtual sample will be more representative of the overall soil mass. Thus fewer failures are expected. The soil mass is also characterized by a smooth field and behaves like a uniform soil that is more accurately represented by traditional theories, thus figure 5.12c illustrates a failure surface that coincides with traditional theory.

For extremely small values of $\Theta_{\ln \tan \phi'}$ the soil mass modeled by the RFEM varies rapidly from point to point (see Figure 5.11a) and a virtual sample is not sufficient to characterize the soil mass. The predicted probability is less than that for an intermediate value of $\Theta_{\ln \tan \phi'}$ due to the fact that local averaging effects begin to dominant and variance reduction is significant at the element level. Additionally, the small value of $\Theta_{\ln \tan \phi'}$ does not allow for larger weak zone in the random field. Without large weak zones, the failure mechanism tends to be more traditional as a path through the weakest soil elements is unlikely as the path is winding. The behavior of the soil is more consistent with traditional theory as illustrated in figure 5.12a where the a larger value of the shear strain invariant along the traditional failure plane is apparent.

Not all realizations for intermediate values of $\Theta_{\ln \tan \phi'}$ produce results as dramatic as figure 5.12b. To illustrate this, the shear strain invariant has been contoured for another realization (see Figure 5.13).



(a)

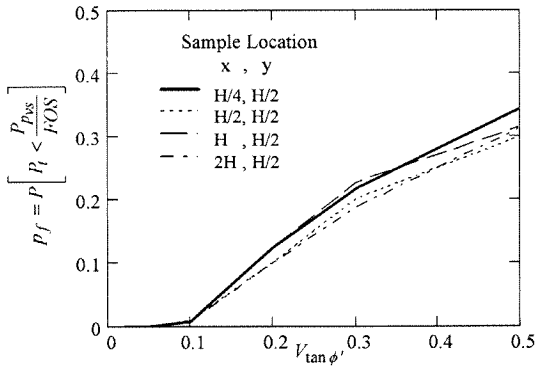
(b)

Figure 5.13: (a) Passive earth displacement for a soil friction angle realization, $V_{\tan\phi'} = 0.5$ and $\Theta_{\ln\tan\phi'} = 0.5$, and (b) corresponding contour of shear strain invariant for a soil friction angle realization.

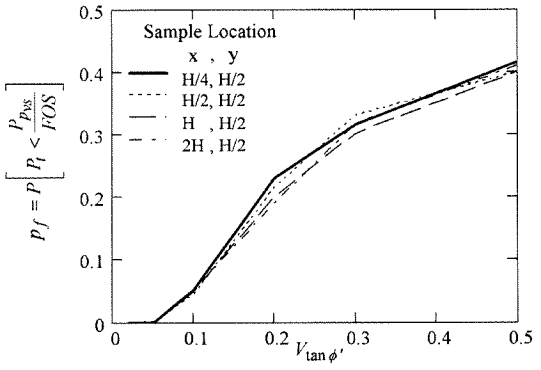
For this realization, the failure mechanism illustrated in figure 5.13b closely resembles that of the traditional failure surface. It is important to note that the input statistics are the same as those used in figures 5.11 and 5.12, but the soil realization and therefore the random field are unique (see Figure 4.3).

The influence of the location of the virtual sample point is illustrated in figure 5.14. There is little influence for very small values of $\Theta_{\ln \tan \phi'}$, where virtual samples do not characterize the soil mass. For intermediate and larger values of $\Theta_{\ln \tan \phi'}$, the probability of failure is minimized for samples located at a horizontal distance between mid height and the total height of the wall.

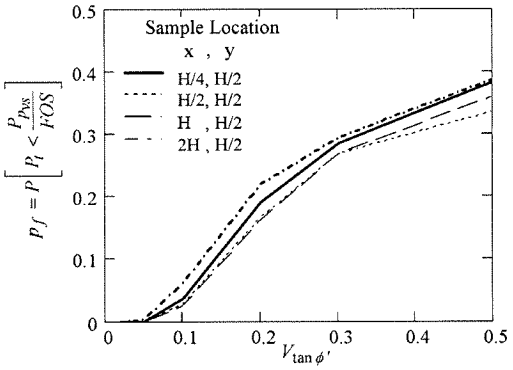
Figure 5.15 illustrates the influence of characterizing the soil based on two virtual sample points. For all values of $\Theta_{\ln \tan \phi'}$, the probability of failure is decreased as the number of virtual sample points is increased and an average soil property obtained from the samples is used to determine $P_{p_{VS}}$. As an example, the probability of failure for $FOS=1.2$ with two sample points located at (H/2, H/2) and (H, H /2), $\Theta_{\ln \tan \phi'} = 0.05$ and $V_{\tan \phi} = 0.5$ is about 25%. For the same parameters and a single sample point located at (H /2, H /2) the probability of failure was about 30%.



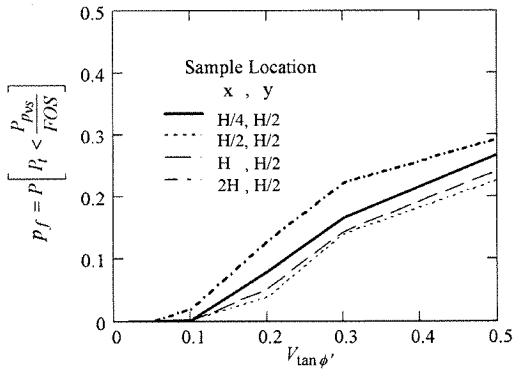
(a) $\Theta_{\ln\tan\phi'} = 0.05$



(b) $\Theta_{\ln\tan\phi'} = 0.2$



(c) $\Theta_{\ln\tan\phi'} = 1.0$



(d) $\Theta_{\ln\tan\phi'} = 5.0$

Figure 5.14: Estimated probability of failure, p_f, that the true lateral passive load will be less than the factored predicted design load for varying virtual sample point locations with *FOS=1.2* and (a) $\Theta_{\ln\tan\phi'} = 0.05$, (b) $\Theta_{\ln\tan\phi'} = 0.2$, (c) $\Theta_{\ln\tan\phi'} = 1.0$, and (d) $\Theta_{\ln\tan\phi'} = 5.0$.

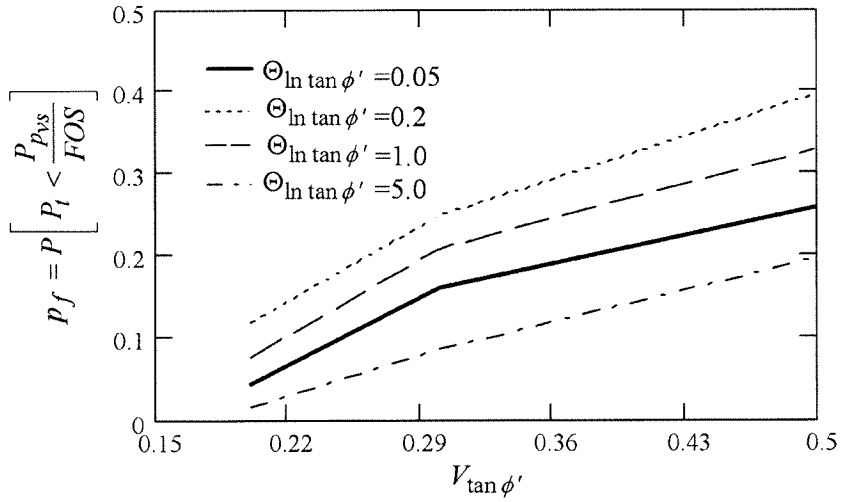


Figure 5.15: Estimated probability of failure, p_f, that the true lateral passive load will be less than the factored predicted design for virtual samples located at (H/2, H/2) and (H, H /2) with FOS=1.2.

5.4 Comparison of the FOSM and the RFEM Methods

The following section will compare the results of the modified FOSM method and the RFEM based on virtual sampling. The results corresponding to a single virtual sample located at (H/2, H/2) will always be presented as a single sample point was shown to produce a more conservative value for the probability of failure.

It is assumed that the RFEM results are a better estimate of the probability of failure as it directly accounts for spatial variability. It does not require the assumption of a probability density function and it has the ability to model non-

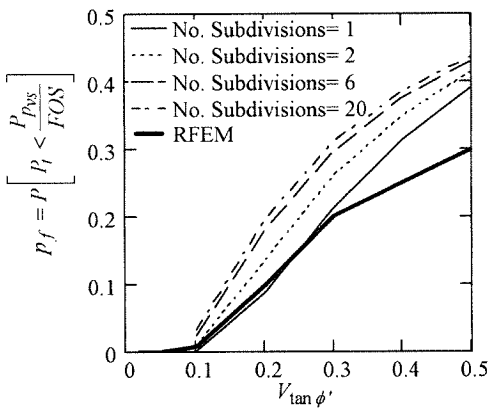
linear performance functions. The RFEM results are used as a benchmark in the following discussions.

5.4.1 Influence of the Coefficient of Variation on Design Reliability

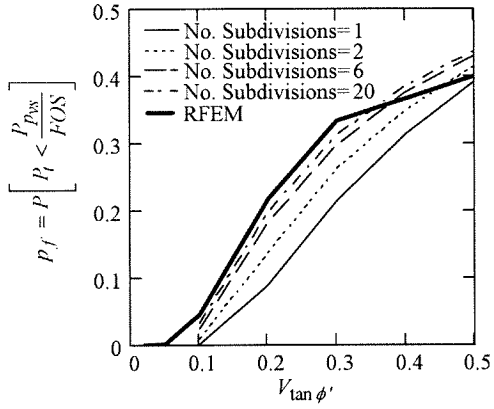
Figure 5.16 indicates that performing local averaging over the entire failure surface may not be conservative for intermediate values of $\Theta_{\ln \tan \phi'}$. The results of the RFEM are better approximated by subdividing the failure surface and reducing the length over which local averaging is taking place.

For large values of $\Theta_{\ln \tan \phi'}$, where the virtually sampled soil property better represents the characteristic soil property, the RFEM produces a lower probability of failure than the modified FOSM method.

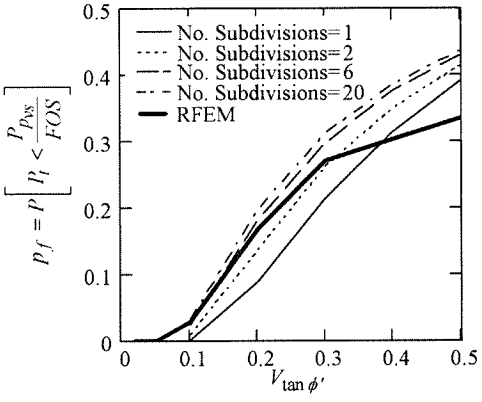
For very small values of $\Theta_{\ln \tan \phi'}$, the RFEM results are dominated by local averaging and the modified FOSM method best approximates the RFEM for the case of performing the local averaging over the entire failure surface.



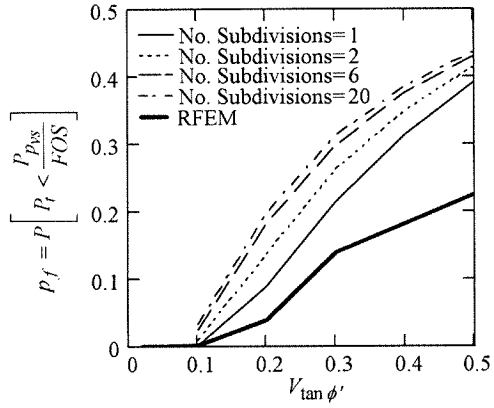
(a) $\Theta_{\ln\tan\phi'} = 0.05$



(b) $\Theta_{\ln\tan\phi'} = 0.2$



(c) $\Theta_{\ln\tan\phi'} = 1.0$



(d) $\Theta_{\ln\tan\phi'} = 5.0$

Figure 5.16: Estimated probability of failure, p_f, that the true lateral passive load will be less than the factored predicted design load with *FOS=1.2* and (a) $\Theta_{\ln\tan\phi'} = 0.05$, (b) $\Theta_{\ln\tan\phi'} = 0.2$, (c) $\Theta_{\ln\tan\phi'} = 1.0$, and (d) $\Theta_{\ln\tan\phi'} = 5.0$.

5.4.2 Influence of Spatial Correlation Length on Design Reliability

Figure 5.17 illustrates that a maximum probability of failure is predicted by the RFEM for intermediate values of $\Theta_{\ln \tan \phi'}$ and for values of $V_{\tan \phi'}$ less the 0.5. The RFEM is more accurately represented by the modified FOSM method when a greater number of subdivisions is used. For a value of $V_{\tan \phi'} = 0.5$, the RFEM and the modified FOSM method, with an increased number of subdivisions, have good agreement.

As the spatial correlation length is increased, the sampled soil properties more accurately estimate the characteristic properties of the soil and the probability of failure is reduced for the RFEM and the results predicted from the modified FOSM method are conservative.

(a) $V_{\tan\phi'} = 0.20$

(b) $V_{\tan\phi'} = 0.30$

(c) $V_{\tan\phi'} = 0.50$

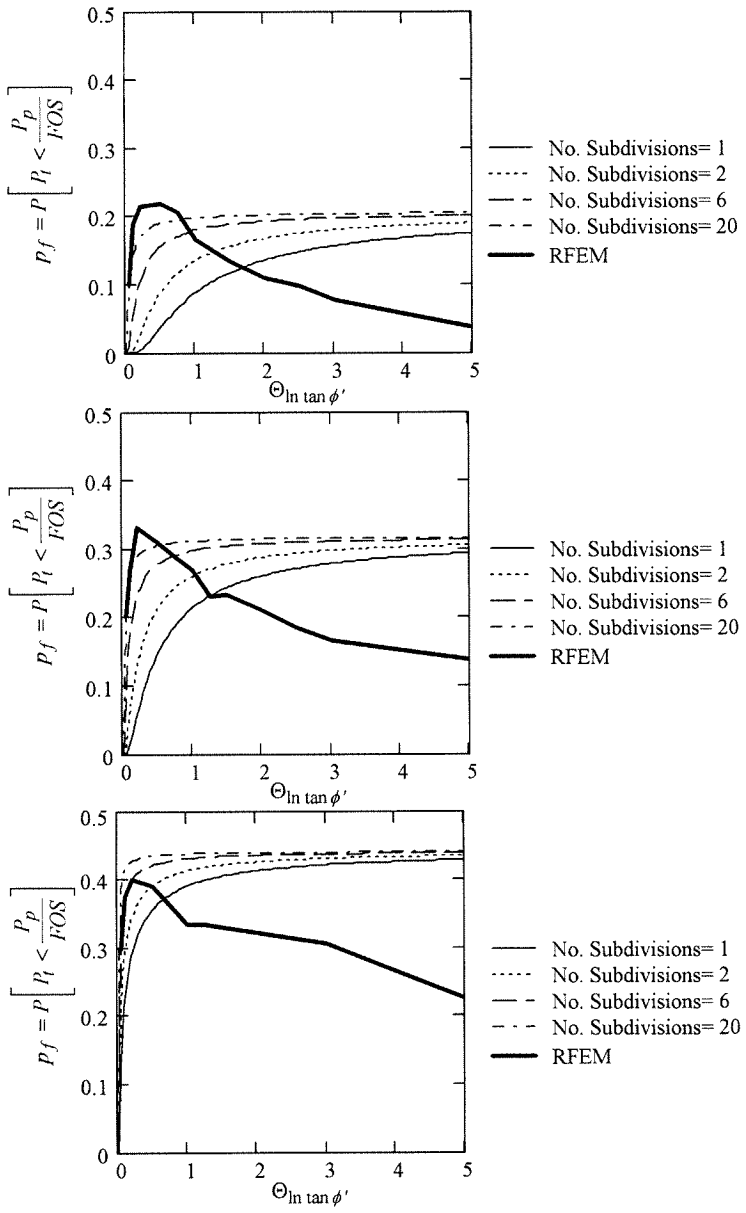


Figure 5.17: Estimated probability of failure, p_f, that the true lateral passive load will be less than the factored predicted design load with *FOS=1.2* and (a) $V_{\tan\phi'} = 0.20$, (b) $V_{\tan\phi'} = 0.30$, (c) $V_{\tan\phi'} = 0.50$.

5.4.3 Summary of Observations

For values of $\Theta_{\ln \tan \phi'}$ close to the critical value, the modified FOSM method can be used to estimate the probability of failure provided the length over which local averaging occurs is small. In other words a large number of subdivisions should be used. A conservative estimate would be to assume an infinite number of subdivisions, corresponding to a value of infinity for $\Theta_{\ln \tan \phi'}$ which implies no local averaging. This assumption would overestimate the probability of failure for spatial variability characterized by a large value of $\Theta_{\ln \tan \phi'}$ where sample soil properties more accurately reflect the characteristic properties of the soil.

6. SLOPE STABILITY

The slope under consideration is shown in Figure 6.1, and consists of undrained clay, with shear strength parameters $\phi'_u = 0$ and c_u.

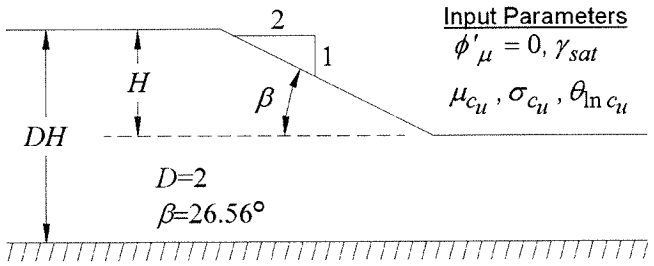


Figure 6.1: Cohesive slope test problem

This is the same test slope considered by Griffiths and Fenton 2004. In this study, the slope inclination and dimensions, give by β, H, and D, and the saturated unit weight of the soil, γ_{sat}, are held constant while the undrained shear strength c_u is assumed to be a random variable. The undrained shear strength is conveniently expressed in the dimensionless form C, where

$$C = \frac{c_u}{\gamma_{sat} H} \tag{6.1}$$

The shear strength, C, is assumed to be characterized statistically by a lognormal distribution defined by a mean, μ_C and a standard deviation, σ_C. The mean and standard deviation can be expressed in terms of the dimensionless coefficient of variation, defined as

$$V_C = \frac{\sigma_C}{\mu_C} \tag{6.2}$$

The third parameter considered is the spatial correlation length, $\theta_{\ln C}$. In this study, the spatial correlation length has been normalized by the height of the slope, H, and will be expressed in the form,

$$\Theta_{\ln C} = \frac{\theta_{\ln C}}{H} \tag{6.3}$$

It has been suggested (see, e.g., Lee et al. 1983; Phoon & Kulhawy 1999) that typical V_C values for undrained shear strength are in the range of 0.1 - 0.5. The spatial correlation length is less well documented and may exhibit anisotropy. Although the capability of modeling an anisotropic soil is available, the spatial correlation considered in this study will be assumed to be isotropic.

The parameters considered in this work are shown in table 6.1.

Parameter	Values Considered
V_C	0.1, 0.5, 1.0
$\Theta_{\ln C}$	0.5, 1.0, 2.0, 4.0, 8.0

Table 6.1: Parameters varied in study

A mean value of $\mu_C = 0.25$, which corresponds to a unit weight of 20 and $c_u = 5.0$ for the slope geometry considered, will be used in this work.

6.1 Traditional Slope Stability Equilibrium Methods

A large number of equilibrium methods are available and are discussed by Duncan and Wright (2005). All equilibrium methods are based on the assumption that the failing soil mass can be divided into slices over a proposed failure surface. To facilitate the solution for the equations of equilibrium, additional assumptions are then by made relating the force directions between the slices. This work uses Bishop's Modified Method of slices (Bishop 1955).

6.1.1 Bishop's Modified Method of Slices

Bishop's Modified Method of Slices is based on a circular failure surface as shown in figure 6.2.

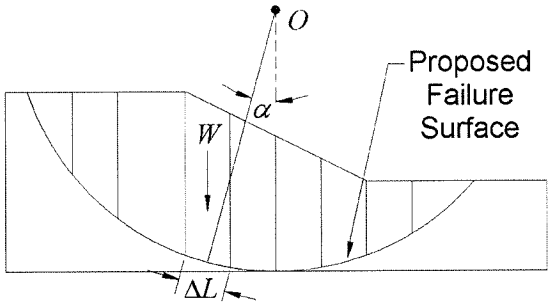


Figure 6.2: Bishop's Modified Method of Slice

The method involves dividing the soil mass into slices, assuming horizontal interslice forces and performing equilibrium on each slice. Failure is assumed to occur by rotation of a block of soil on a cylindrical slip surface centered on O (see Figure 6.2). By examining overall moment equilibrium about O an expression for the factor of safety is obtained. For the test problem considered, with shear strength parameters $\phi'_u = 0$ and c_u, the expression for the factor of safety FOS is

$$FOS = \frac{\sum c_u \Delta L}{\sum W \sin \alpha} \tag{6.4}$$

where ΔL and W are the length and weight of each slice, respectively and α is the slice angle as shown in figure 6.2.

The method is iterative in that, the correct solution is the proposed failure circle that gives the minimum FOS.

For the slope shown in figure 6.1, the factor of safety was obtained using Bishop's Modified Method to give the data in table 6.2.

C	FOS
0.15	0.88
0.17	1.00
0.20	1.18
0.25	1.47
0.30	1.77

Table 6.2: FOS Assuming a Homogeneous Soil

The data from table 6.2 is shown graphically in figure 6.3.

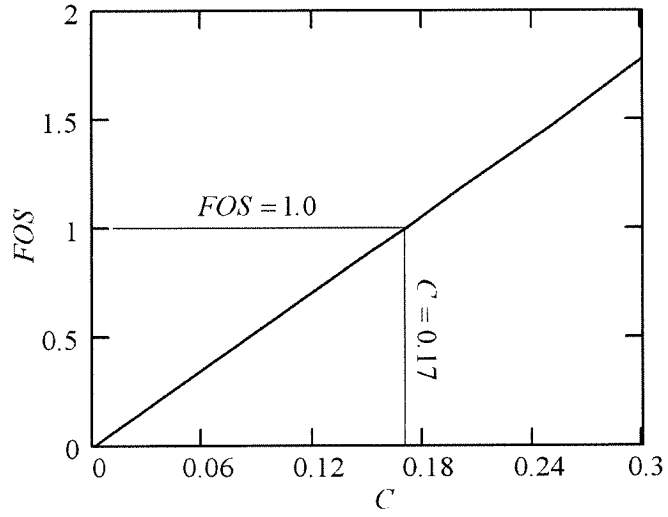


Figure 6.3: Linear relationship between FOS and C for a cohesive slope with $\beta = 26.67°$ and D=2.

Figure 6.3 shows a linear relationship exists between the FOS and C. The equation for the FOS can thus be represented as

$$FOS = \frac{1.0}{0.17} C = 5.88 C \tag{6.5}$$

6.2 First Order Second Moment (FOSM) Method

The FOSM method will be performed assuming the performance function is defined by equation 6.5. Therefore, the mean value of the FOS, using equation 3.1, is defined by

$$\mathrm{E}[FOS] = \mu_{FOS} \cong 5.88\, \mu_C \tag{6.6}$$

The variance, using equation 3.2, is defined by

$$\mathrm{VAR}[FOS] = \sigma^2{}_{FOS} \cong (5.88)^2\, \sigma^2{}_C \tag{6.7}$$

The modified method that accounts for spatial correlation will be used, therefore the values used in equation 6.6 and 6.7 will be adjusted due to local averaging. The failure surface over which local averaging will be performed is the failure circle that produced the minimum FOS determined using Bishop's Modified Method.

The failure circle will be subdivided into equal arc lengths (see Figure 6.4) and the soil properties will be locally averaged along each arc length, S_A.

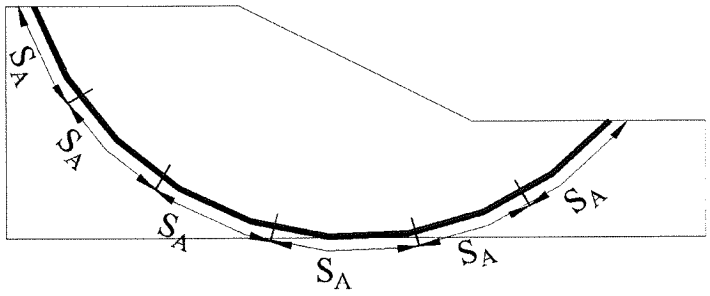


Figure 6.4: Assumed Failure Circle with Example Subdivisions

The locally averaged arc length is defined by

$$S_A = \frac{Failure\,Circle\,Arc\,Length}{Number\,of\,Subdivisions} \tag{6.8}$$

The locally averaged arc length, S, is synonymous $\alpha\theta$. The relationship between the number of subdivisions and $\alpha\theta$ is illustrated in figure 6.5.

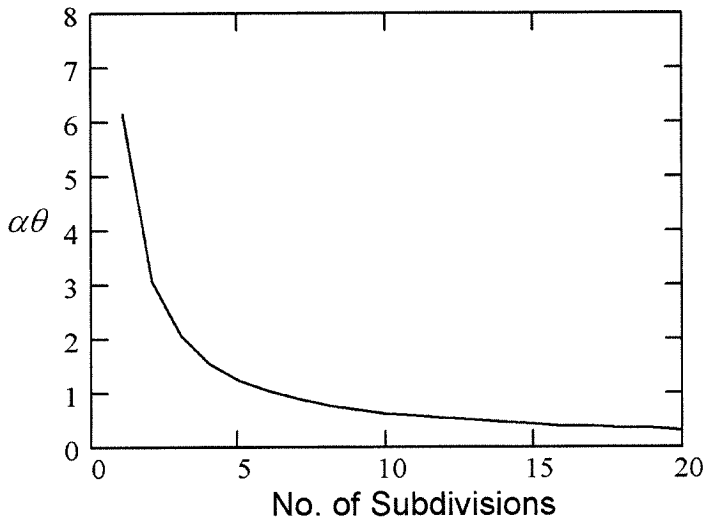


Figure 6.5: $\alpha\theta$ vs. Number of Subdivisions

6.2.1 Variance Reduction Due to Local Averaging

The influence of the number of subdivisions on the locally averaged statistics, normalized by the input statistics, is illustrated in Figure 6.6.

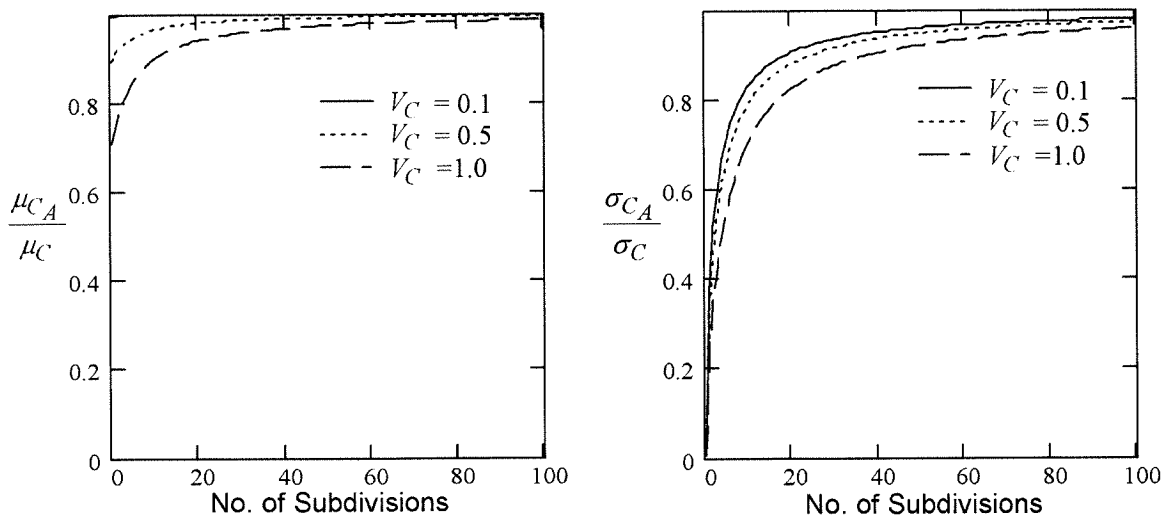


Figure 6.6: Influence of number of subdivisions on local averaging: influence on the (a) mean and (b) standard deviation for $\Theta_{\ln C} = 1.0$.

Figure 6.6 illustrates that for larger numbers of subdivisions, the locally averaged statistics approach the input statistics. A large number of subdivisions indicate that the arc length over which local averaging is occurring is small with respect to the spatial correlation length and the locally averaged statistics closely resemble the input point statistics. A fewer number of subdivisions indicate that the arc lengths are large with respect to the spatial correlation length and the locally averaged statistics are reduced. As the number of subdivisions approaches zero, the locally averaged mean approaches the median value (see Equation 3.9) of the input statistics and the standard deviation tends toward zero. This observation corresponds with the results from the previously presented passive earth pressure analysis.

6.2.2 Design Reliability

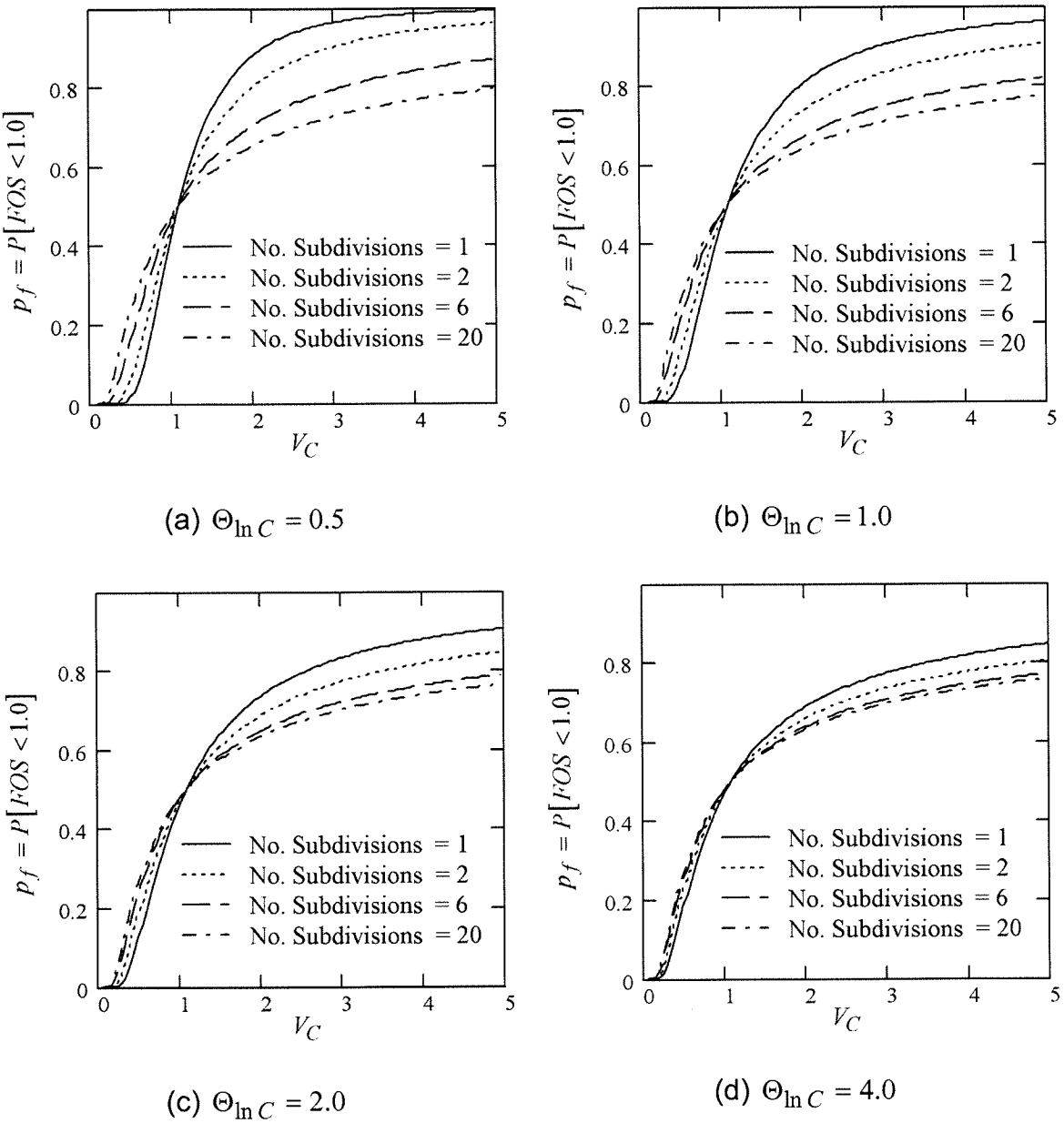
The slope is assumed to have failed if the FOS is equal to one. Therefore the probability of failure is defined by

$$p_f = P[FOS < 1.0] \tag{6.9}$$

where FOS is as defined by Equation 6.6. The form of the probability density function is assumed to be lognormal.

6.2.3 FOSM Method Results

Figure 6.7 illustrates the influence of V_C and the number of subdivisions on the estimated probability of failure.



(a) $\Theta_{\ln C} = 0.5$

(b) $\Theta_{\ln C} = 1.0$

(c) $\Theta_{\ln C} = 2.0$

(d) $\Theta_{\ln C} = 4.0$

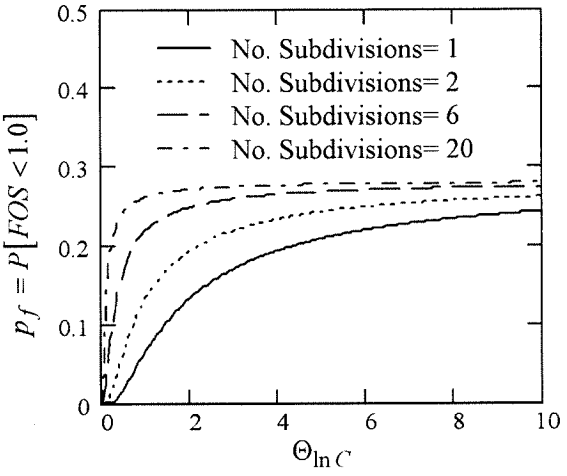
Figure 6.7: Estimated probability of failure, p_f vs. the coefficient of variation, V_C for (a) $\Theta_{\ln C} = 0.5$, (b) $\Theta_{\ln C} = 1.0$, (c) $\Theta_{\ln C} = 2.0$, and (d) $\Theta_{\ln C} = 5.0$.

All curves cross over at a critical value of $V_C = 1.08$. This is the value of V_C which results in the $Median_C = 0.17$ (see Equation 3.9) and from table 6.2 a $FOS = 1.0$. This result is similar to the study presented by Griffiths and Fenton (2004) where a critical value of V_C was determined by performing variance reduction over a square element.

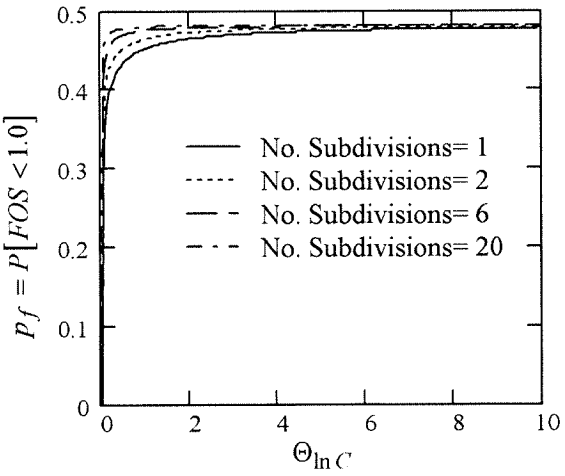
The estimated probability of failure associated with the critical value of V_C is $p_f = 0.50$.

For values of $V_C < 1.08$, the probability of failure increases with the number of subdivisions. For values of $V_C > 1.08$, the probability of failure decreases with the number of subdivisions.

The influence of $\Theta_{\ln C}$ and the number of subdivisions on the estimated probability of failure is better illustrated by figure 6.8.



(a) $V_C = 0.5$



(b) $V_C = 1.0$

Figure 6.8: Estimated probability of failure, p_f vs. the spatial correlation length , $\Theta_{\ln C}$ for
(a) $V_C = 0.5$ and (b) $V_C = 1.0$.

Figure 6.8 illustrates that the impact of the number of subdivisions on the estimated probability of failure is not influenced for values of V_C near the critical value. For values of V_C sufficiently less than the critical value, the estimated probability of failure is increased as the number of subdivisions increases.

From figure 6.8, it can be observed that the probability of failure reaches a maximum value as the correlation length increases. The maximum value is that which would be obtained assuming no local averaging, which implies a spatially uniform soil or a spatial correlation length equal to infinity. The estimated probability of failure assuming $\Theta_{\ln C} = \infty$ is shown in figure 6.9.

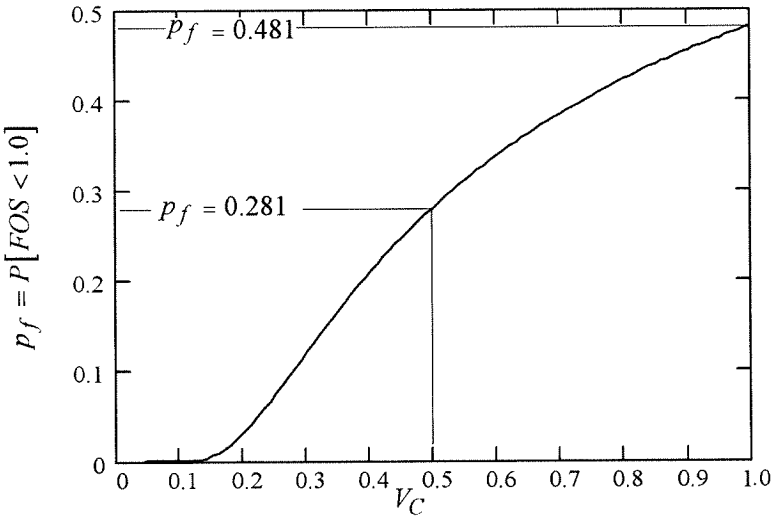


Figure 6.9: Estimated probability of failure, p_f vs. the coefficient of variation, V_C for $\Theta_{\ln C} = \infty$.

6.3 Random Finite Element Method (RFEM)

The soil mass is discretized into 910 square, eight node finite elements as show in figure 6.10. Each element has a side length of 0.1. Units are not used as the results are applicable to any consistent set of units.

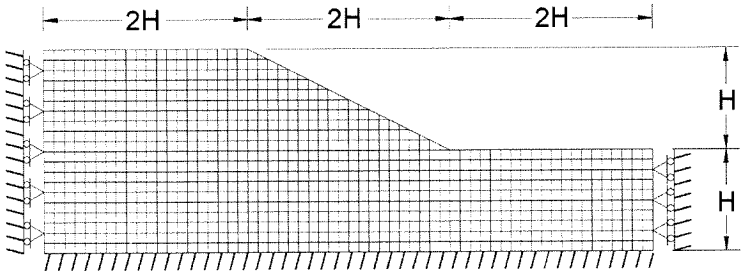


Figure 6.10: Mesh Used for Random Finite Element Slope Stability Analysis

The finite element model used in this study includes the soil dilation angle, taken to be zero, Poisson's ratio, taken to be 0.3 and Young's modulus, taken to be 1×10^5. These properties are assumed to be spatially constant. The unit weight is a function of the shear strength parameter (see Equation 6.1) and is assumed to be spatially constant.

The study will assume that C is a log-normally distributed field.

6.3.1 Design Reliability

For a given set of input shear strength parameters (μ_C, σ_C, $\theta_{\ln C}$), 1000 simulations are performed for each set of input parameters. The probability of failure is defined as the proportion of 1,000 Monte Carlo slope stability analyses

failed. In this study, failure is said to have occurred if, for any given realization, the finite element algorithm was unable to converge within 500 iterations.

6.3.2 Monte Carlo Results

Figure 6.11 illustrates the influence of V_C on the estimated probability of failure for several values of $\Theta_{\ln C}$.

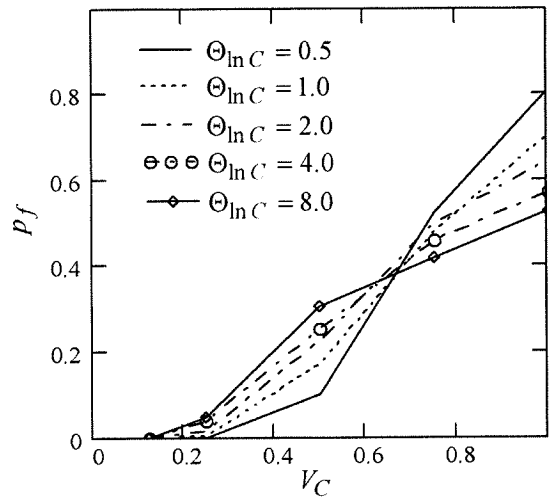


Figure 6.11: Estimated probability of failure, p_f, vs. the coefficient of variation, V_C.

Similar to figure 6.7, figure 6.11 illustrates a value for V_C where the curves tend to cross over. For the RFEM, the critical value is $0.65 < V_C < 0.70$, which corresponds to an estimated probability of failure of $0.35 < p_f < 0.5$.

For values of $V_C < 0.65$, the probability of failure increases for larger values of $\Theta_{\ln C}$. For values of $V_C > 0.70$, the probability of failure decreases for larger values of $\Theta_{\ln C}$.

The influence of $\Theta_{\ln C}$ on the estimated probability of failure is also illustrated by figure 6.12.

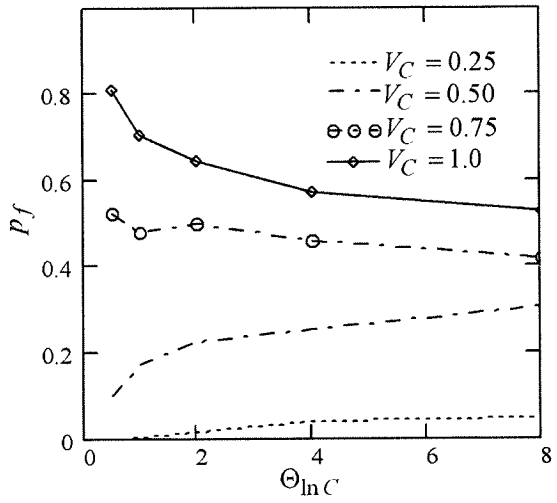


Figure 6.12: Estimated probability of failure, p_f, vs. the spatial correlation length, $\Theta_{\ln C}$.

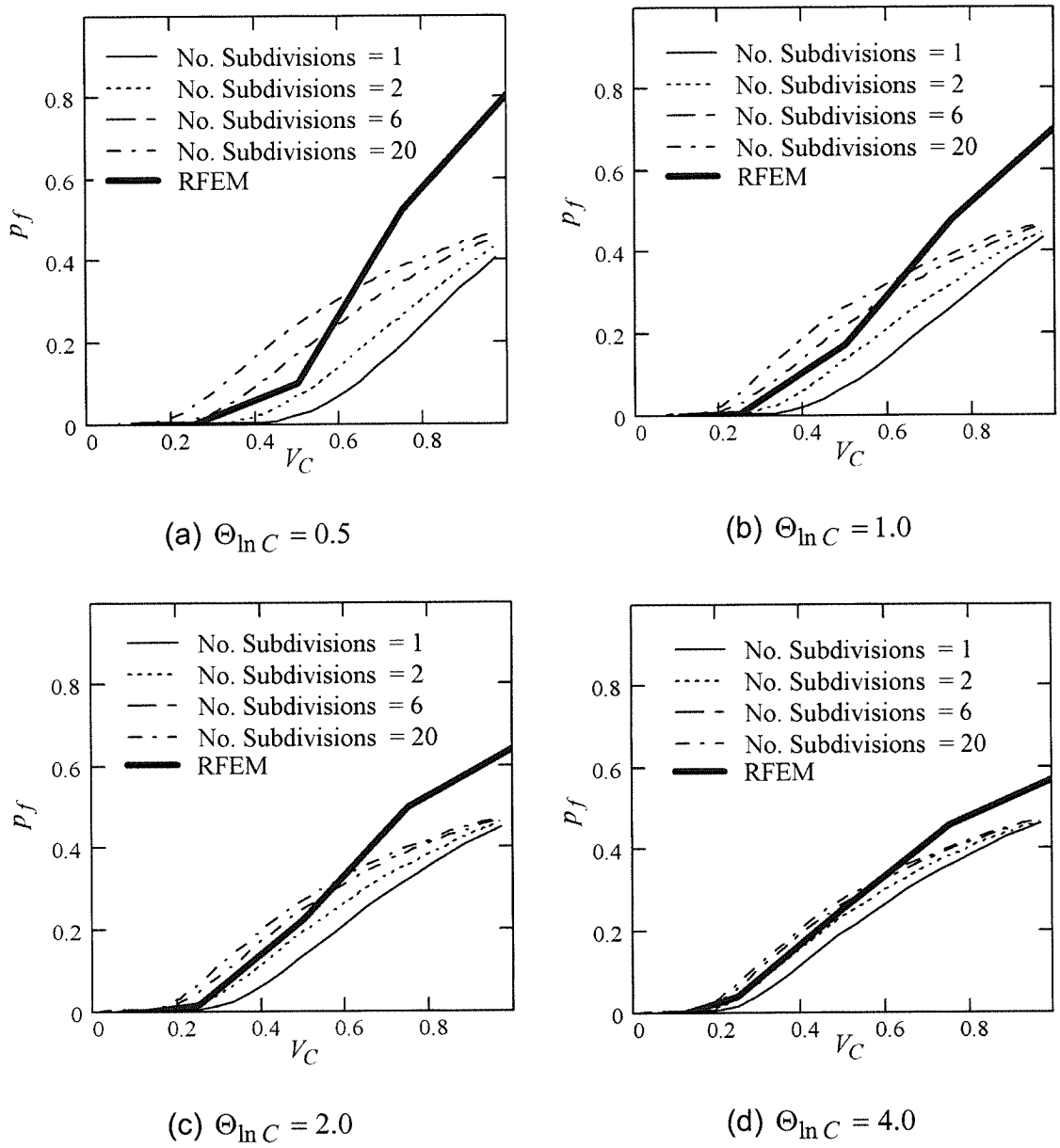
6.4 Comparison of the FOSM and the RFEM Methods

The following section will compare the results of the modified FOSM method and the RFEM. It is assumed that the RFEM results are a better estimate of the probability of failure as it directly accounts for spatial variability. It does not require the assumption of a probability density function and it has the ability to model non-linear performance functions. The RFEM results are used as a benchmark in the following discussions.

Figure 6.13 illustrates that the modified FOSM method underestimates the probability of failure for higher values of V_C regardless of the number of subdivisions.

For lower values of V_C, the modified FOSM method overestimates the probability of failure and gives conservative results compared to the RFEM provided the number of subdivisions is greater than 2.

In all cases, as $\Theta_{\ln C}$ increases, the RFEM and the modified FOSM method begin to converge. This is more clearly represented in figure 6.14.



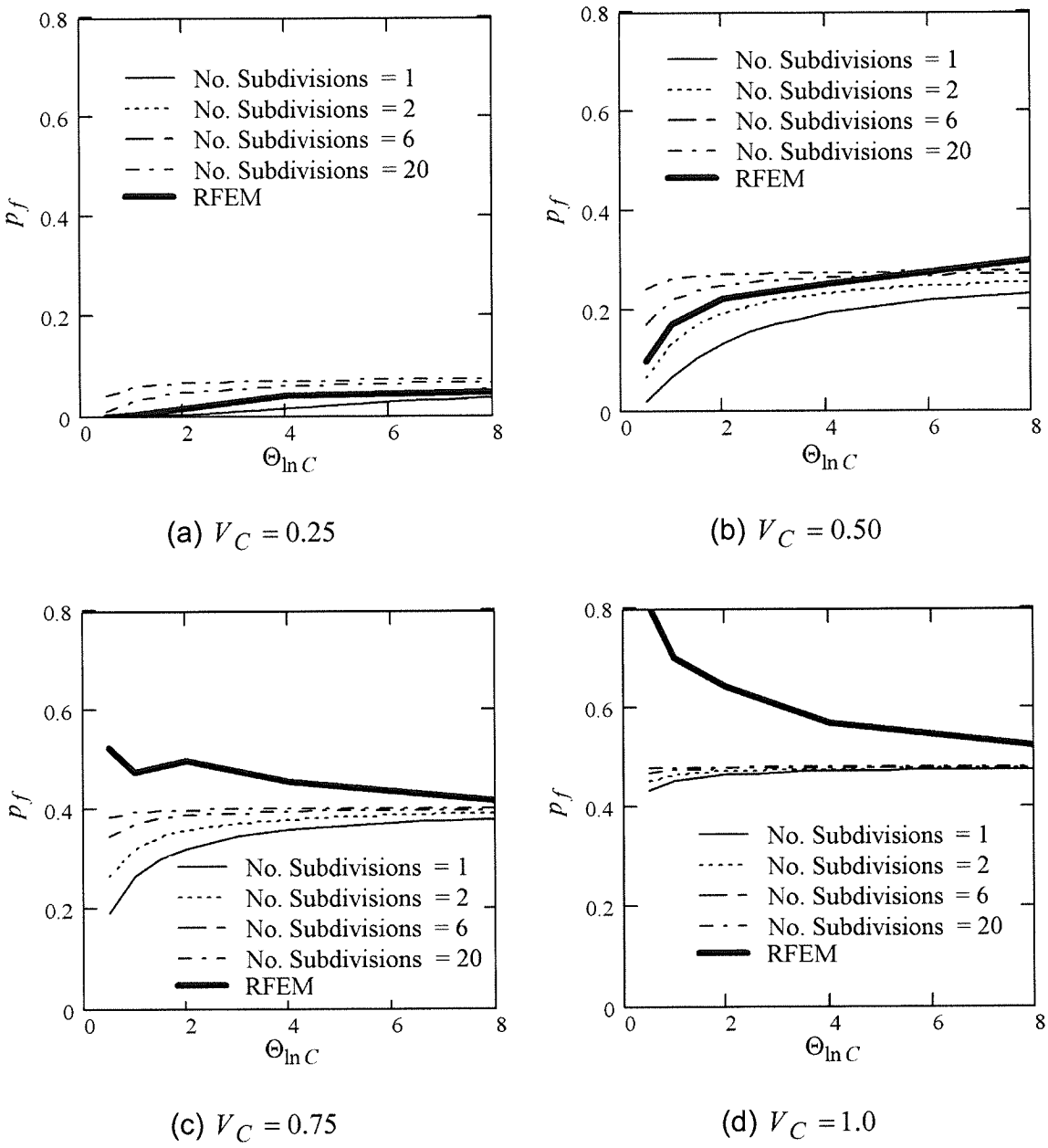
(a) $\Theta_{\ln C} = 0.5$

(b) $\Theta_{\ln C} = 1.0$

(c) $\Theta_{\ln C} = 2.0$

(d) $\Theta_{\ln C} = 4.0$

Figure 6.13: Estimated probability of failure, p_f vs. the coefficient of variation, V_C for (a) $\Theta_{\ln C} = 0.5$, (b) $\Theta_{\ln C} = 1.0$, (c) $\Theta_{\ln C} = 2.0$, and (d) $\Theta_{\ln C} = 4.0$.



(a) $V_C = 0.25$

(b) $V_C = 0.50$

(c) $V_C = 0.75$

(d) $V_C = 1.0$

Figure 6.14: Estimated probability of failure, p_f vs. the coefficient of variation, V_C for (a) $V_C = 0.25$, (b) $V_C = 0.50$, (c) $V_C = 0.75$, and (d) $V_C = 1.0$.

Figure 6.14 clearly shows the two methods converging as $\Theta_{\ln C}$ increases. For both solution methods, the convergence is tending towards the value that would be obtained assuming no local averaging, which implies a spatially uniform soil or a spatial correlation length equal to infinity. The estimated probability of failure assuming $\Theta_{\ln C} = \infty$ is shown in figure 6.9.

6.4.1 Summary of Observations

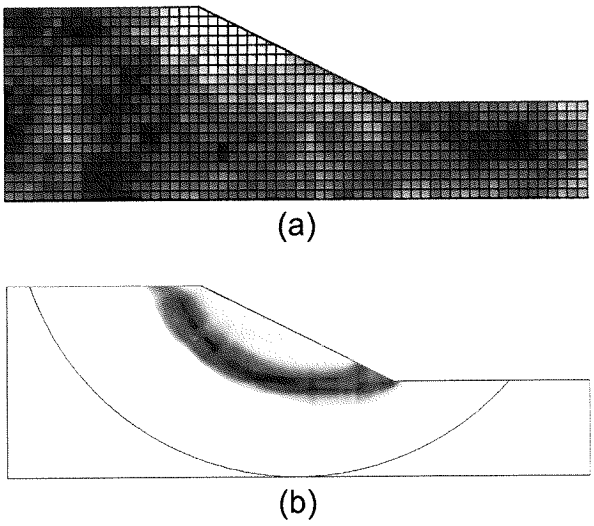
For large values of $\Theta_{\ln C}$, the modified FOSM and the RFEM methods have good agreement. This is due to the fact that as $\Theta_{\ln C}$ increases, the soil becomes increasingly uniform. A solution technique that assumes a spatially uniform soil, like the FOSM method, would therefore produce an accurate estimate of the probability of failure.

For smaller values of $\Theta_{\ln C}$, say $\Theta_{\ln C} < 4.0$, the agreement between the modified FOSM method and the RFEM is dependent on the degree a shear strength variability.

For values of $V_C > 0.50$, the modified FOSM method was not conservative when compared to the RFEM regardless of the length over which local averaging was occurring. This is due to the fact that the failure surface assumption required for the modified FOSM method may not always be accurate.

The RFEM does not require a failure surface assumption and the soil is allowed to fail along the weakest path. For larger values of V_C, sufficiently weaker zones are possible within the slope (see Figure 6.15a). The failure surface of the slope will tend towards the weaker zones and will not resemble the failure surface as assumed by the modified FOSM method. This is illustrated in

figure 6.15b, where the shear strain invariant has been contoured at failure for a single Monte Carlo realization.



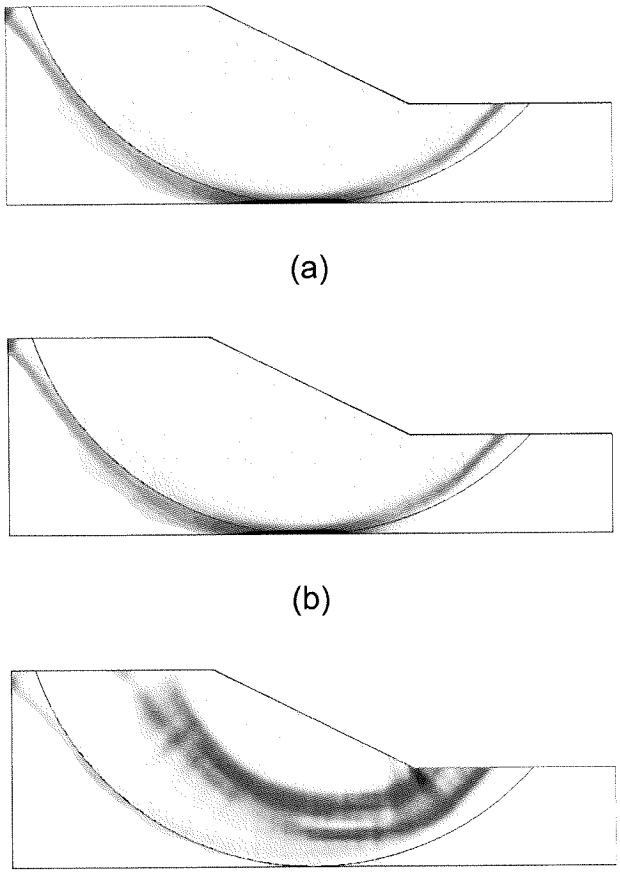
(a)

(b)

Figure 6.15: (a) Soil shear strength realization grey scale plot, $V_C = 1.0$ and $\Theta_{\ln C} = 4.0$, and (b) corresponding contour of shear strain invariant at failure.

For values of $V_C < 0.50$, the RFEM produced conservative values of the estimated probability of failure with respect to the modified FOSM method when the number of subdivisions was greater than 2. This is due to the fact that although weaker zones of soil form within the random field, they are not sufficiently weak to allow a failure mechanism to be mobilized in these regions.

For example, for the realization shown in figure 6.15, the slope analyzed by the RFEM does not fail when $V_C = 0.25$. The failure that is typical for $V_C = 0.25$ is characterized by that defined by Bishop's method as illustrated in figure 6.16.



(a)

(b)

(c)

Figure 6.16: Contour of shear strain invariant at failure for different Monte Carlo realizations with $V_C = 0.25$ and $\Theta_{\ln C} = 4.0$.

Figure 6.16 shows the shear strain invariant at failure for three different Monte Carlo simulations with $V_C = 0.25$ and $\Theta_{\ln C} = 4.0$. The FOSM method failure surface is included on the plots for comparison. Figure 6.16a and 6.16b show a failure mechanism that strictly follows that used in the modified FOSM method assumed failure circle. Figure 6.16c illustrates the formation of two failure mechanisms, one that follows the assumed failure circle and one that deviates from it.

Although the formation of a failure mechanism different than that assumed in the modified FOSM method is formed, the inclusion of the assumed failure surface means that the FOSM method assumption is reasonably valid. Due to the assumed failure mechanism following that allowed by the RFEM, the estimated probability of failure for lower values of V_C using the modified FOSM method with a sufficient number of subdivisions corresponds with the RFEM solution. This is due to the performance function more accurately representing the performance of the slope. The modified FOSM method could therefore be used to estimate the probability of failure for a slope with $V_C < 0.50$.

The requirement of the additional knowledge regarding the appropriate number of subdivisions to be used with the modified FOSM method identifies the RFEM as the appropriate method for determining the estimated probability of failure for lower values of V_C.

7. CONCLUDING REMARKS AND FUTURE WORK

7.1 Concluding Remarks

The estimated probability of failure for a spatially variable soil has been investigated using the modified FOSM method and RFEM for both a passive earth pressure analysis and a slope stability analysis. The modified FOSM method required the definition of a performance function to characterize the behavior of the soil. The RFEM did not require any assumptions regarding the behavior of the soil.

For both analyses, as the soil became increasingly variable, the estimated probability of failure increased.

For larger spatial correlation lengths, the soil tends to perform as defined by traditional equilibrium theory. The traditional equilibrium theories were developed assuming uniform soil properties and for larger spatial correlation length, the soil is essentially uniform. The modified FOSM method had better agreement with the RFEM as the assumed performance function more accurately represented the actual soil behavior.

For smaller spatial correlation lengths it was shown that the soil tends to behave more like that defined using traditional equilibrium theory. The modified FOSM method had better agreement with the RFEM as the performance function more accurately represented the actual soil behavior.

For intermediate values of the spatial correlation length the modified FOSM method and the RFEM method did not have good agreement. It was shown that for intermediate values the failure surface did not always correspond with that defined by traditional equilibrium theory. The performance function

assumed in the modified FOSM method did not model the soil behavior in this case.

7.2 Suggestions for Future Work

The influence of anisotropic spatial correlation lengths on the estimated probability of failure should be investigated. This solution when compared to the isotropic solution would identify if there is a significant need to include anisotropic soil behavior. If anisotropic spatial correlation length significantly influences the estimated probability of failure, additional investigation regarding the horizontal relationship would be required.

Develop a 3-D RFEM method. This solution when compared to the 2-D solution would identify if variability in 3-D influences the estimated probability of failure. This investigation would allow one to assess if the additional computational time required for a 3-D analysis would be required to better estimate the probability of failure.

7.2.1 Passive Earth Pressure

Further Investigate the influence of 'virtual sample' locations and quantities of samples used to characterize the soil on the estimated probability of failure. This analysis would provide information regarding the benefit of additional sight investigations that would better characterize the soil shear strength parameters.

7.2.2 Slope Stability Analysis

Investigate the influence on the estimated probability of failure determined using the modified FOSM method and different slope stability theories. This solution would modify the performance function used in this work and indicate if an alternate slope stability theory would better estimate the probability of failure.

Using the RFEM, investigate the probability of failure of existing failed slope geometries. This information could be used to further validate the RFEM as the preferred method for estimating the probability of failure.

REFERENCES CITED

[1] Baecher, G. B. and Christian, C. T. (2003). *Reliability and statistics in geotechnical engineering*, Wiley, Chichester, U. K.

[2] Cherubini, C. (2000). Reliability evaluation of shallow foundation bearing capacity on *c', ϕ'* soils. *Can. Geotech. J.*, 37, 264-269.

[3] Christian, J. T., Ladd, C. C., & Baecher, G. B. (1994). Reliability applied to slope stability analysis. *J. Geotech. Eng.*, 120(20). 2180-2207.

[4] Chowdhury, R. N. & Tang, W. H. (1987). Comparison of risk models for slopes. *Proc., 5th Int. Conf. on Applications of Statistics and Probability in Soil and Structural Engineering*, 2, 863-869.

[5] Cormeau, I. C. (1975). Numerical stability in quasi-static elasto-viscoplasticity. *Int. J. Numer. Methods Eng.*, 9(1), 109-127.

[6] Cornell, C. A. (1969). Structural safety specifications based on second moment reliability analysis. Dept. of Civil Engineering, Massachusetts Institute of Technology, Cambridge, Mass.

[7] Duncan, J. M. & Wright, S. W. (2005). *Soil strength and slope stability*. John Wiley & Sons, Inc., Hoboken, New Jersey.

[8] Duncan, J. M. (2000). Factors of safety and reliability in geotechnical engineering. *J. Geotech. Geoenviron. Eng.*, 126(4), 307-316.

[9] El-Ramly, H., Morgenstern, N. R., & Cruden, D. M. (2002). Probabilistic slope stability analysis for practice. *Can Geotech. J.*, 39, 665-683.

[10] Fenton, G. A. (1999a). Estimation for stochastic soil models. *J. Geotech. Geoenviron. Eng.*, 125(6), 470-485.

[11] Fenton, G. A. (1999b). Random field modeling of CPT data. *J. Geotech. Geoenviron. Eng.*, 125(6), 486-498.

[12] Fenton, G. A., & Griffiths, D. V. (1993). Statistics of flow through a simple bounded stochastic medium. *Water Resour. Res.*, 29(6), 1825-1830.

[13] Fenton, G. A., & Griffiths, D. V. (1996). Statistics of free surface flow through stochastic earth dam. *J. Geotech. Geoenviron. Eng.*, 122(6), 427-436.

[14] Fenton, G.A. & Griffiths, D.V. (2003). Bearing capacity of spatially raondom c-ϕ soils. *Can. Geotech. J.* 40(1), 54-65.

[15] Fenton, G.A, Griffiths, D.V., & Williams, M.B. (2005). Reliability of traditional retaining wall design. *Geotechnique* 55(1), 55-62.

[16] Fenton, G. A. & Vanmarcke, E. H. (1990). Simulation of random fields via local average subdivision. *J. Eng. Mech.*, 116(8), 1733-1749.

[17] Griffiths, D. V. (1980). Finite element analyses of walls, footings and slopes. *Proceedings of a symposium on computer applications to geotechnical problems in highway engineering*, Cambridge, UK, pp. 122-146.

[18] Griffiths, D. V., & Fenton, G. A. (2001). Bearing capacity of spatially random soil: The undrained prandtl problem revisited. *Geotechnique*, 51(4), 351-359

[19] Griffths, D. V. & Fenton, G. A. (2004). Probabilistic slope stability analysis by finite elements. *J. Geotech. Geoenviron. Eng.*, 130(5), 507-518.

[20] Griffiths, D. V. & Lane, P. A. (1999). Slope stability analysis by finite elements. *Geotechnique*, 49(3), 387-403.

[21] Hoeksema, R. J. & Kitanidis, P. K. (1985). Analysis of the spatial structure of properties of selected aquifers. *Water Resour. Res.*, 21(4), 563-572.

[22] Jaky, J. (1944). The coefficient of earth pressure at rest. *J. Soc. Hung. Archit. Engrs,* 355-358.

[23] Lacasse, S., & Nadim, R. (1996). Uncertainties in characterizing soil properties. *Uncertainty in the geological environment: Soil Properties, Geotechnical Special Publication No. 58*, C. D. Shackelford et al., eds., ASCE, New York, 49-75.

[24] Lee, I. K., White, W., & Ingles, O. G. (1983). *Geotechnical engineering.*, Pitman, London.

[25] Li, K. S. & White, W. (1987). Probabilistic characterization of soil profiles. *Research Report No. 19*. Dept. Civil Engg, University College, Uni NSW, Canberra, ACT.

[26] Li, K. S. & Lumb, P. (1987). Probabilistic design of slopes. *Can Geotech. J.*, 24, 520-531.

[27] Lumb, P. (1966). The varaiblity of natural soils. *Can. Geotech. J.,* Vol III, 2, 74-94.

[28] Matsuo, M. & Kuroda, K. (1974). Probabilistic approach to the design of embankments. *Soils Found.* 14(1), 1-17.

[29] Mostyn, G. R. & Li, K. S. (1993). Probabilistic slope stability-State of play. *Proc., Conf. on Probabilistic Methods in Geotechnical Engineering*, K. S. Li and S. C. R. Lo, eds., Balkema, Rotterdam, The Netherlands.

[30] Peck, R. B. (1969). Ninth Rankine lecture: Advantages and limitations of the observational method in applied soil mechanics. *Geotechnique*, 19(2), 171-187.

[31] Peschl, G. M. & Schweiger, H. F. (2003). Reliability analysis in geotechnics with finite elements. Comparison of probabilistic, stochastic and fuzzy set methods. In *ISIPTA ' 03*. Lugano, Switzerland, 437-451.

[32] Perzyna, P. (1966). Fundamental problems in viscoplasticity. *Adv. Appl. Mechanics*. 9, 243-377.

[33] Phoon, K. & Kulhawy, F. H. (1999). Characterization of geotechnical variability. *Can. Geotech. J.* 36, 612-624.

[34] Rosenblueth, E. (1975). Point estimates for probability moments. *Proc. Natl. Acad. Sci.* U.S.A., 72(10), 3812-3814.

[35] Rosenblueth, E. (1981). Two-point estimates in probabilities. *Appl. Math. Model.* 5(2), 329-335.

[36] Smith, I. M. and Griffiths, D. V. (2004). *Programming the finite element method, 4th Ed.* Wiley, Chichester, U. K.

[37] Sudicky, E. A. (1986). A natural gradient experiment on solute transport in a sand aquifer: Spatial variability of hydraulic conductivity and its role in the dispersion process. *Water Resour. Res.,* 23(13), 2069-2083.

[38] Tang, W. H., Yucemen, M. S., & Ang, A. H. S. (1976). Probability-based short-term design of slopes. *Can. Geotech. J.,* 13, 201-2115.

[39] Terzagi, K. (1929). Effect of minor geological details on the stability of dams. *Technical Publication No. 215*, American Institute of Mining and Metallurgical Engineers, New York, 31-44.

[40] Vanmarke, E. H. (1984). *Random fields: Analysis and synthesis.* MIT Press, Cambridge, Mass.

[41] Wolf, T.F. (1996). Probabilistic slope stability in theory and practice. *Uncertainty in the geological environment: From theory to practice, Geotechnical Special Publication No. 58*, C. D. Shackelford et al., eds., ASCE, New York, 419-433.

[42] Ziekiewicz, O. C. & Cormeau, I. C. (1974). Viscoplasticty, plasticity and creep in elastic solids. a unified approach. *Int. J. Numer. Methods Eng.*, 8, 821-845.